



**FEDERAL UNIVERSITY OF MINAS GERAIS**  
**Engineering School**  
**Postgraduate Program in Mechanical Engineering**

**LUCAS AMARAL COSTA**

**DEVELOPMENT OF AN INTELLIGENT PARKING DUPLICATOR  
MECHANICAL DEVICE**

Belo Horizonte

2019



Lucas Amaral Costa

## **DEVELOPMENT OF AN INTELLIGENT PARKING DUPLICATOR MECHANICAL DEVICE**

### **Final version**

Master's thesis submitted to the Department of Mechanical Engineering of the Federal University of Minas Gerais, in partial fulfillment of the requirements for the degree of Masters of Science in Mechanical Engineering.

Concentration Area: Projects and Systems

Research Area: Machinery Design

Advisor: Prof. PhD. Alessandro Corrêa Victorino

Belo Horizonte

2019

C837d	<p>Costa, Lucas Amaral.  Development of an intelligent parking duplicator mechanical device [recurso eletrônico] / Lucas Amaral Costa. - 2019.  1 recurso online (98 f. : il., color.) : pdf.</p> <p>Orientado: Alessandro Corrêa Victorino.</p> <p>Dissertação (mestrado) - Universidade Federal de Minas Gerais, Escola de Engenharia.</p> <p>Apêndices: f. 96-98.</p> <p>Bibliografia: f. 93-95.</p> <p>Exigências do sistema: Adobe Acrobat Reader.</p> <p>1. Engenharia mecânica - Teses. 2. Automóveis - Estacionamento - Teses. 3. Método dos elementos finitos - Teses. 4. Sistemas especialistas (Computação) - Teses. I. Victorino, Alessandro Corrêa. II. Universidade Federal de Minas Gerais. Escola de Engenharia. III. Título.</p> <p style="text-align: right;">CDU: 621 (043)</p>
-------	------------------------------------------------------------------------------------------------------------------------------------------------------------------------------------------------------------------------------------------------------------------------------------------------------------------------------------------------------------------------------------------------------------------------------------------------------------------------------------------------------------------------------------------------------------------------------------------------------------------------------------------------------------------------------------------------------------------------------------------------------------------------------------------------------------



**UNIVERSIDADE FEDERAL DE MINAS GERAIS**  
**PROGRAMA DE PÓS-GRADUAÇÃO EM**  
**ENGENHARIA MECÂNICA**

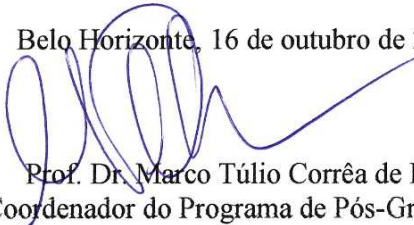
Av. Antônio Carlos, 6627 - Campus Universitário  
31270-901 - Belo Horizonte - MG  
Tel.: +55 31 3409.5145  
E-mail: [cpgmec@demec.ufmg.br](mailto:cpgmec@demec.ufmg.br)

## **ATESTADO**

Atesto, para os devidos fins, que **Lucas Amaral Costa**, defendeu, aos 16 de outubro de 2019, às 15:30 horas, perante Banca Examinadora homologada pelo Colegiado do Programa de Pós-Graduação em Engenharia Mecânica da Universidade Federal de Minas Gerais, constituída pelos professores: Alessandro Correa Victorino - Orientador - Departamento de Engenharia Mecânica/ UFMG, Dimas Abreu Archanjo Dutra/ Departamento de Engenharia Mecânica/ UFMG, Danilo Amaral/ Departamento de Engenharia Mecânica/ UFMG, a dissertação intitulada "**DEVELOPMENT OF AN INTELLIGENT PARKING DUPLICATOR MECHANICAL DEVICE**".

**Salientamos que o Sr. Lucas Amaral Costa estará apto a gozar dos direitos que o referido título lhe concede, somente após a obtenção do Certificado de Conclusão do Mestrado. Este certificado será emitido pelo Programa de Pós-Graduação em Engenharia Mecânica após a entrega, pelo mestrando, da versão final da dissertação, atendendo às exigências da Banca Examinadora.**

Belo Horizonte, 16 de outubro de 2019.

  
Prof. Dr. Marco Túlio Corrêa de Faria  
Coordenador do Programa de Pós-Graduação  
em Engenharia Mecânica da UFMG



To my parents, brother and friends.

## **ACKNOWLEDGMENTS**

First and foremost I would like to thank God, who guided my steps through the ways of success.

Thank my parents, Jairo and Amariles; my brother, Leandro; my girlfriend Stela; all the family members and friends, who gave me strength, support and encouragement with great affection. It was worth it. All the distance, all the suffering, all the renunciations.

A special thanks to Pedro, Eurico, uncle Gê, Samuel, Estevão and Bernardo, who helped in the best way they could.

Thank all the professors, colleagues and friends, very important in my academic life, for the daily living, for the constant help and for all the shared teachings.

Thank my advisor, Prof. PhD. Alessandro Corrêa Victorino, for the opportunity, patience in the mentoring, support and incentive, making possible the conclusion of this master's thesis.

The author is also grateful for the support of Programa de Pós-Graduação da Universidade Federal de Minas Gerais, Coordenação de Aperfeiçoamento de Pessoal de Nível Superior (CAPES), Fundação de Amparo à Pesquisa do Estado de Minas Gerais (FAPEMIG), Conselho Nacional de Desenvolvimento Científico e Tecnológico (CNPq) and Fundação de Desenvolvimento da Pesquisa (Fundep) in the development of the present academic work.

My sincere thanks.

*“The mind that opens up to a new idea never returns to its original size.”*

– Albert Einstein.

## NOTE

The present dissertation is a thesis by published works, i.e., it is a collection of the research papers (COSTA, 2017), (COSTA e VICTORINO, 2019), (COSTA e VICTORINO, 2018), (COSTA, COSTA, *et al.*, 2017) and (COSTA, VICTORINO e CHAVES, 2020). The master's student is the main author of all these papers. This format was chosen because it offers a series of advantages, as stated in (WRITING A THESIS AS A COLLECTION OF PAPERS, 2016):

- The student graduates with more published papers in the master's degree, which also improves skills such as writing, selecting and responding to reviewers' comments;
- The examiner is presented with a work that has already been peer reviewed and is above a certain quality standard;
- The thesis is submitted in a shorter period than by the traditional structure. This work was submitted in a shorter time than the 24 months required for the master's degree.

It is important to note that the student did the change of level from the master to the doctorate. According to the current regulations, the change of level must be done within 18 months since the entrance in the program.

## ABSTRACT

As in (JUNIOR, ALENCAR e JOHN, 2011) and (A proporção de habitantes por carro nas capitais, 2016), the extensive increase in the fleet of vehicles in urban centers brings the challenge of parking several vehicles in confined spaces. A possible solution to this problem is the development of high-tech parking systems capable of parking multiple vehicles in limited spaces. The current thesis presents a solution to this problem and consists of developing a parking duplicator device that allows parking two vehicles in the space required to park only one. The solution is to lift one of the vehicles so that the other one can occupy the space below it. The device's development was achieved by means of stress-strain analysis and CAD/CAM techniques. First, the design characteristics of the parking system were defined, and a conceptual design was developed. The structural analysis was then performed. The obtained results were used in the dimensioning of the elements determining its dimensions. Next, the solutions were refined through finite element analysis. Finally, a virtual prototype and a detailed project were developed mainly in the software SOLIDWORKS® v. 2019. And a reduced scale prototype was 3D printed. The obtained structure was a simple and inexpensive solution optimizing the parking system. The proposed device presents simple and innovative configuration and drive (with movable pulley) besides the characteristic of being able to be easily manufactured and assembled in series, which provides lower final cost of the product and characterizes it, along with its other attributes, as a great invention compared to the similar equipment currently available on the market, hitherto patented or in the state of the art. A patent application was deposited under the registration number BR1020170118142.

*Keywords: Parking Duplicator. Second Class Lever. Movable Pulley. Shear Pin. Stress-Strain Analysis. Finite Element Analysis. Intelligent System.*

## RESUMO

Tal como em (JUNIOR, ALENCAR e JOHN, 2011) e (A proporção de habitantes por carro nas capitais, 2016), o grande aumento da frota de veículos nos centros urbanos traz o desafio de estacionar vários veículos em espaços confinados. Uma possível solução para este problema está no desenvolvimento de sistemas de estacionamento de alta tecnologia capazes de estacionar múltiplos veículos em espaços limitados. A presente dissertação apresenta uma solução para este problema e consiste no desenvolvimento de um dispositivo duplicador de estacionamento que permite estacionar dois veículos no espaço necessário para estacionar apenas um. A solução é levantar um dos veículos, para que o outro possa ocupar o espaço abaixo dele. O desenvolvimento do dispositivo foi realizado por meio de análises de tensão-deformação e técnicas de CAD/CAM. Primeiro, as características de projeto do sistema de estacionamento foram definidas e um projeto conceitual foi desenvolvido. Então a análise estrutural foi realizada. Os resultados obtidos foram utilizados no dimensionamento dos elementos determinando as suas dimensões. Em seguida as soluções foram refinadas através da análise de elementos finitos. Por fim, um protótipo virtual e um projeto detalhado foram desenvolvidos principalmente no software SOLIDWORKS® v. 2019. E um protótipo em escala reduzida foi impresso em 3D. A estrutura obtida foi uma solução simples e de baixo custo otimizando o sistema de estacionamento. O dispositivo proposto apresenta configuração e acionamento simples e inovador (com polia móvel) além das característica de poder ser facilmente fabricado e montado em série, o que proporciona menor custo final do produto acabado e o caracteriza, juntamente com seus demais atributos, como uma grande invenção em comparação com os equipamentos similares atualmente disponíveis no mercado, até então patenteado ou no estado da arte. Um pedido de patente foi depositado sob o número de registro BR1020170118142.

*Palavras-chave: Duplicador de Estacionamento. Alavanca Inter-Resistente. Roldana Móvel. Pino de Cisalhamento. Análise de Tensão-Deformação. Análise de Elementos Finitos. Sistema Inteligente.*



## LIST OF FIGURES

Figure 1 - Patent 9906103-1A .....	23
Figure 2 - Patent 0002843-6 A .....	24
Figure 3 - Patent US 5110250 A .....	25
Figure 4 - Stress–strain curve .....	26
Figure 5 - Permissible stress according to Bach.....	27
Figure 6 - Effective length factors .....	29
Figure 7 - Class 2 lever.....	30
Figure 8 - Movable pulley .....	31
Figure 9 - Shaft with static loading .....	32
Figure 10 - Sheet metals 1 and 2 .....	37
Figure 11 - Strain on the sheet metals .....	37
Figure 12 - Grid supporting the sheet metals .....	38
Figure 13 - Dimensions of the grid.....	39
Figure 14 - Grid structural analysis in the software MASTAN2® exhibiting the bending moment.....	44
Figure 15 - Load on the Pivots and Pillars .....	48
Figure 16 - Parking maneuver onto the platform .....	51
Figure 17 - Parking duplicator device as a second-class lever .....	57
Figure 18 – Selection of steel cable.....	63
Figure 19 – Force One 3D printer of the company 3D LAB.....	66
Figure 20 - Technical specifications of the Force One 3D printer .....	67
Figure 21 - Labor cost estimate. ....	71
Figure 22 - Virtual prototype developed for the duplicator.....	72
Figure 23 - Device’s general operation. ....	73
Figure 24 - Parking duplicator view. ....	74
Figure 25 - Side view of the parking duplicator.....	75
Figure 26 - Alternative assembly (dimensions in mm). ....	75
Figure 27 - Upper bound axial and bending (N/m <sup>2</sup> ). ....	77
Figure 28 - FEA with a beam 100x100x8 mm .....	78
Figure 29 - Main dimensions of the grid .....	79
Figure 30 - Small-scale 3D printed prototype. ....	80
Figure 31 - Electronic circuit of the mini gearmotor.....	82
Figure 32 - Location of cameras and sensor.....	85
Figure 33 - Parking maneuver. ....	86

## LIST OF TABLES

Table 1 - Technical Details.....	76
Table 2 - Technical details of the mini gearmotor.....	80
Table 3 - Cost Estimate (R\$).....	87
Table 4 - Cost Estimate (\$).....	88

## **LIST OF SYMBOLS**

<i>FEM</i>	Finite Element Methods
<i>CAD</i>	Computer Aided Design
<i>CAE</i>	Computer Aided Engineering

## NOMENCLATURE

### Latin Letters

$E$	Elastic modulus of the material
$I_{xx}$	Moment of inertia in relation to x-axis
$w_v$	Distributed load of the vehicle
$w_{\#}$	Distributed load of the sheet metal
$W$	Resistance module
$a$	Length of the fold of the sheet metal
$M$	Bending moment
$h$	Distance between the center of mass and the most distant fiber
$R$	Reaction force
$Q$	Load
$d$	Distance
$f_{cr}$	critical buckling stress
$P$	Power
$v$	Velocity of the lift platform
$P_{ef}$	Effective power of the gearmotor
$I$	Reduction rate
$SEW f_e$	Service factor of the gearmotor
$m$	Mass
$F_0$	Force to elevate the load on the lift platform
$P_{ef}$	Effective power of the gearmotor
$F_A$	Real force necessary to raise the load
$F_R$	Retention force necessary to hold the load when lowering the platform
$V_F$	Speed of the steel cable
$CT$	Work load on the steel cable
$d_c$	Diameter of the steel cable
$D_p$	Diameter of the pulley
$D_p$	Diameter of the pulley's shear pin
$R_1$	Support reaction 1
$R_2$	Support reaction 2

$R_3$	Support reaction 3
$\sum M_i$	Sum of the moments in relation to a point
$\sum V_i$	Sum of the vertical forces
$\sum H_i$	Sum of the horizontal forces

## Greek Letters

$\delta_{\text{máx}}$	Maximal arrow
$\alpha$	Angle
$\tau$	Shear Stress
$\eta$	Efficiency in raising the load



# CONTENTS

ABSTRACT .....	8
RESUMO.....	9
LIST OF FIGURES .....	10
LIST OF TABLES.....	11
NOMENCLATURE .....	13
1 INTRODUCTION .....	18
1.1 Publications .....	20
2 OBJECTIVES.....	22
3 LITERATURE REVIEW .....	23
3.1 Patent 9906103-1A .....	23
3.2 Patent 0002843-6 A .....	24
3.3 Patent US 5110250 A .....	25
3.4 Limit of elastic/plastic behavior .....	25
3.5 Dimensioning of machine parts .....	27
3.6 Shear pin .....	28
3.7 Buckling.....	29
3.8 Class 2 lever.....	30
3.9 Movable pulley .....	31
3.10 Support reactions .....	32
3.10.1 First condition: $\sum M_i = 0$ .....	32
3.10.2 Second condition: $\sum V_i = 0$ .....	33
3.10.3 Third condition: $\sum H_i = 0$ .....	33
3.10.4 Statically indeterminate .....	33
4 METHODS.....	34
4.1 Design Characteristics and Sketch .....	34
4.2 Conceptual Design.....	35
4.3 Analytical Dimensioning.....	35
4.3.1 Folded sheet metal .....	36
4.3.2 Grid.....	43
4.3.2 Pivots .....	47
4.3.3 Pillar.....	54
4.3.4 Gearmotor.....	57
4.3.5 Steel Cable.....	59
4.3.7 Pulley .....	64
4.3.6 Minimum diameter for the pulley's shear pin .....	64
4.3.7 Ball bearing plummer block unit.....	65
4.4 Finite Element Analysis (FEA) .....	65
4.5 Virtual Prototype .....	65
4.6 Small-Scale 3D printed Prototype .....	65

4.7	Aid & Security Intelligent System.....	68
4.7.1	Selection of the proper sensor and cameras.....	68
4.7.2	Definition of the optimal location for the sensor and cameras.....	69
4.7.3	Simulation on the software Blensor® .....	69
4.7.4	Development of the Algorithm.....	70
4.8	Cost Estimate.....	70
5	RESULTS AND DISCUSSIONS .....	72
5.1	Virtual Prototype .....	72
5.2	Grid.....	77
5.2	Small-scale 3D printed Prototype.....	79
5.3	Aid & Security Intelligent System.....	82
5.3.1	Selection of the proper sensor and cameras.....	83
5.3.2	Definition of the optimal location for the sensor and cameras.....	83
5.3.3	Simulation on the software Blensor® .....	85
5.5	Cost Estimate.....	86
6	NOTES .....	89
7	CONCLUSION .....	90
	SUGGESTIONS FOR FUTURE WORK .....	92
	REFERENCES .....	93
	APPENDIX A - Drawing 1 .....	96
	APPENDIX B – Drawing 2.....	97
	APPENDIX C – Drawing 3.....	98

## 1 INTRODUCTION

According to a survey of the Polytechnic School of the University of São Paulo (Poli) based on data from the real estate market since 1930, about 25% (or one quarter) of the entire area built in the city is used for parking slots (JUNIOR, ALENCAR e JOHN, 2011). The large number of vehicles in urban centers, such as in the city of São Paulo with 2.2 inhabitants/car in the year of 2016 (A proporção de habitantes por carro nas capitais, 2016), has caused the problem of the need for parking spaces for an increasing number of vehicles in reduced spaces.

A solution to this problem is found in the parking duplicator device of the present discussion. Already in the 3rd century BC, the Greek philosopher Archimedes presented the concept of the simple machines suggesting objects that facilitate the execution of different day to day tasks and which are the basis for the more complex machines created by mankind throughout history. The device in the present discussion is a combination of four of the simple machines: the lever, the inclined plane, the pulley and the wheel & axle. It has a simple form, has the property of being manufactured in an industrial production line, in series, and has as its application field the residential garages (mainly apartment buildings and houses) and commercial garages (such as parking lots and offices).

The vertical parking device is an efficient innovation for the suchlike devices currently available on the market. The device counts with a lift platform, an electric hoist and a movable pulley. It has a lifting platform that allows parking two automobiles in the same area required to park only one automobile. Also, in order to facilitate parking by freeing up the maneuver area, its lift platform has only three fixities (instead of four), i.e., one of its corners is hanging. Hence, the lift platform is formed by a structural steel grid dimensioned to sustain all the strain on the platform. The device also counts with Intelligent Transport Systems (ITS) solutions, developed to assist the driver in the parking maneuver guiding each step of the parking task and avoiding collisions, similarly to an autonomous vehicle. The proposed device is a combination of simplicity in the assembly and state-of-the-art attributes.

There are currently some companies in Brazil that produce parking duplicators. Suchlike devices have been patented. For example, the devices in the patents PI 9906103-1A of 11/18/1999 (RIBEIRO e ALBUQUERQUE, 1999), PI 0002843-6A of 6/14/2000 (CHAGAS,

2000) and US 5110250A of 12/18/1990 (KUO, 1990) present a drive formed by electro-hydraulic, electro-mechanical or manual assemblies. Patents PI 9906103-1A of 11/18/1999 and PI 0002843-6A of 06/14/2000 for example, have a smart design but do not present the platform with only three fixities.

Generally, the majority of duplicators found in the market use hydraulic or electro-mechanical spindle drive system and therefore do not rely on the simplicity of the assembly and the drive of the device proposed here. The present study becomes convenient and necessary since the currently manufactured duplicators do not have the same innovations, drive and configuration presented here and therefore do not display the gains described in this document such as the hanging platform, which has only three fixities, and the energy savings required for raising the vehicle in the second class lever system, for example. In this sense, the presented parking duplicator brings a series of innovations to the current state-of-the-art of similar devices currently available on the market. Thus, a patent application was deposited under the registration number BR1020170118142.

All the mechanical components of the device are dimensioned in this thesis. First it is done a bibliographic review in order to bring better understanding of the current state-of-the-art and to allow better understandings of the science involved in the development of the device. Then it approaches the development of the basic idea of the project, the conceptual design, the calculations, analysis, the virtual prototype developed in the software SOLIDWORKS® v. 2019, a reduced scale 3D printed prototype and the development of the aid system that assists the driver in the maneuver of parking, like an autonomous vehicle.

The obtained results demonstrated that the project conforms to the expected specifications allowing the development of a product that can be widely used in urban centers conceiving wide parking possibilities. The methodology applied in the project development of the present discussion demonstrated to be efficient and so it can be applied to the development of virtually any mechanical design.

## 1.1 Publications

The current introduction was adapted from (COSTA, 2017), (COSTA, COSTA, *et al.*, 2017), (COSTA e VICTORINO, 2018), (COSTA e VICTORINO, 2019) and (COSTA, VICTORINO e CHAVES, 2020), studies written by the author of this thesis.

As the introduction, the whole dissertation was produced from papers written while developing the present project. This methodology was adopted since the publication of papers is very positive for the Master's Degree and so the time was better used in the writing of papers that were afterwards put together forming the present dissertation. These papers are listed below. The first paper listed below is a patent request deposited on June 2017. The second one is an article published on Brazilian Technology Symposium 2017 (BTSym'17). The third one is an article published as a book chapter with the publisher Springer. The fourth one is an article published on Brazilian Technology Symposium 2018 (BTSym'18). The fifth one is not published yet, it is an article that was submitted to the Brazilian Technology Symposium 2019 (BTSym'19) and it will probably be a book chapter with the publisher Springer like the third paper listed below.

COSTA, L. A. **Dispositivo Duplicador de Vagas de Garagem**. BR 10 2017 011814 2, 2 June 2017.

COSTA, L. A. et al. Development of a Parking Duplicator Mechanical Device Driven with Pulley. **Brazilian Technology Symposium (BTSym'17)**, Campinas, 2017. Disponivel em: <<http://lcv.fee.unicamp.br/images/BTSym-17/Papers/72182.pdf>>. ISSN: 2447-8326.

COSTA, L. A.; VICTORINO, A. C. Stress-Strain Analysis of a Parking System's Grid. **Brazilian Technology Symposium (BTSym'18)**, Campinas, 2018. Disponivel em: <<http://lcv.fee.unicamp.br/images/BTSym18/Papers/025.pdf>>. ISSN: 2447-8326.

COSTA, L. A.; VICTORINO, A. C. Stress-Strain Analysis and Optimization of a Parking Duplicator Hanging Grid. In: IANO, Y., et al. **Proceedings of the 4th Brazilian Technology Symposium (BTSym'18) - Emerging Trends and Challenges in Technology**. Campinas: Springer International Publishing, v. 140, 2019. p. 319-327. Disponivel em: <[https://link.springer.com/chapter/10.1007/978-3-030-16053-1\\_31](https://link.springer.com/chapter/10.1007/978-3-030-16053-1_31)>. ISBN: 9783030160524.

COSTA, L. A.; VICTORINO, A. C.; CHAVES, P. A. D. Development of an Intelligent Parking Aid System. In: YUZO IANO, R. A. O. S. G. K. R. P. F. **Proceedings of the 5th Brazilian Technology Symposium: Emerging Trends, Issues, and Challenges in the Brazilian Technology**. Campinas: Springer International Publishing, 2020. Accepted paper. Expected publication to 2020.



## 2 OBJECTIVES

The objective of this thesis is the development of an innovative parking duplicator device capable of lifting vehicles up to 2,000 Kg. Thus, some specific objectives can be proposed:

- Dimensioning of the mechanical components of the parking duplicator device;
- Development of a virtual prototype for the device on the software SOLIDWORKS® v. 2019;
- Development of a reduced scale 3D printed prototype;
- Development of an aid system composed by Intelligent Transport Systems (ITS) solutions that assist the driver in the parking maneuver guiding each step of the parking task and avoiding collisions, similarly to an autonomous vehicle;
- Development of a cost estimate for the device;

### 3 LITERATURE REVIEW

In order to produce new knowledge in a field of science, it is important to understand what has already been produced and what are the boundaries that have to be overcome. Thus, the present section presents a literature review providing this information, besides the theory in which the mechanical device is grounded.

#### 3.1 Patent 9906103-1A

Figure 1 exhibits the Patent 9906103-1A (RIBEIRO e ALBUQUERQUE, 1999). The vehicle to be elevated parks on a platform which is elevated in an electro-hydraulic or electro-mechanical drive. The platform has support arms and rotatory axels, providing an angle of inclination in the upper vehicle relatively to the vehicle that is parked underneath the first one.

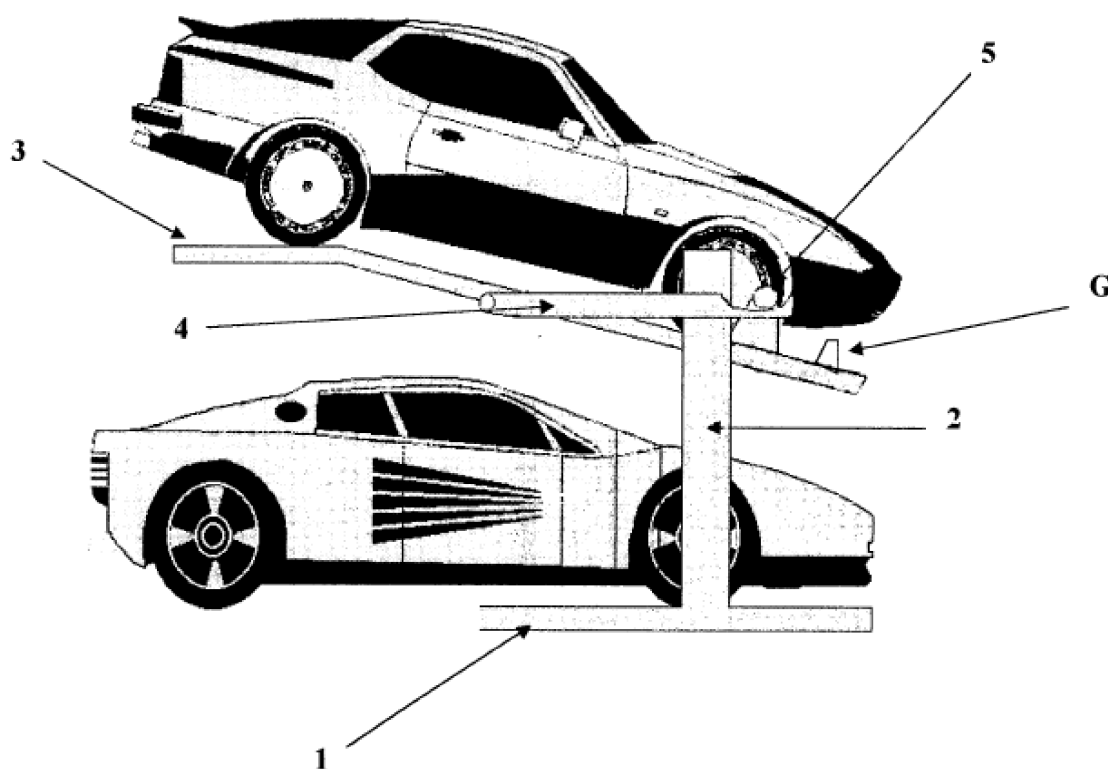


Figure 1 - Patent 9906103-1A

Source: (RIBEIRO e ALBUQUERQUE, 1999).

It is interesting to notice that a second-class lever mechanism, as proposed in the device of the present thesis, would result in a similar angular inclination of the upper vehicle and would confer energy savings as well.

### 3.2 Patent 0002843-6 A

Figure 2 exhibits the Patent 0002843-6 A (CHAGAS, 2000). The first vehicle parks on a platform which is inclined and elevated by an electro-mechanical drive providing free room for the second vehicle to park underneath the first one.

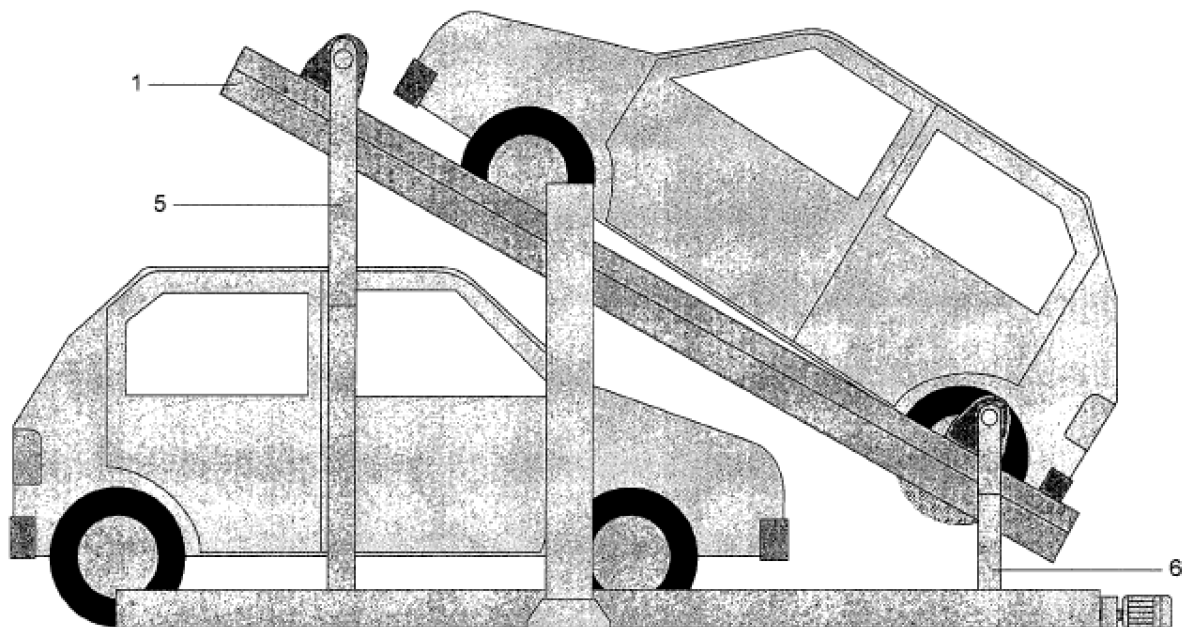


Figure 2 - Patent 0002843-6 A

Source: (CHAGAS, 2000).

It is interesting to notice that the device works a second-class lever in the mechanism that inclines the upper vehicle. But as shown on Figure 2, the two vehicles occupy greater length than it would be required to park only one vehicle as the vehicle underneath does not occupy the entire space underneath the upper vehicle in the case presented.

### 3.3 Patent US 5110250 A

Figure 3 exhibits the Patent US 5110250 A (KUO, 1990). The device supports two vehicles, one above and another underneath it. In order to park the upper vehicle, the elevated platform has a telescopic mechanism that with a retractable ramp for the vehicle to drive over to the upper parking space. The telescopic mechanism is also articulated by pulleys. The drive of the telescopic mechanism can be manual or electro-mechanical.

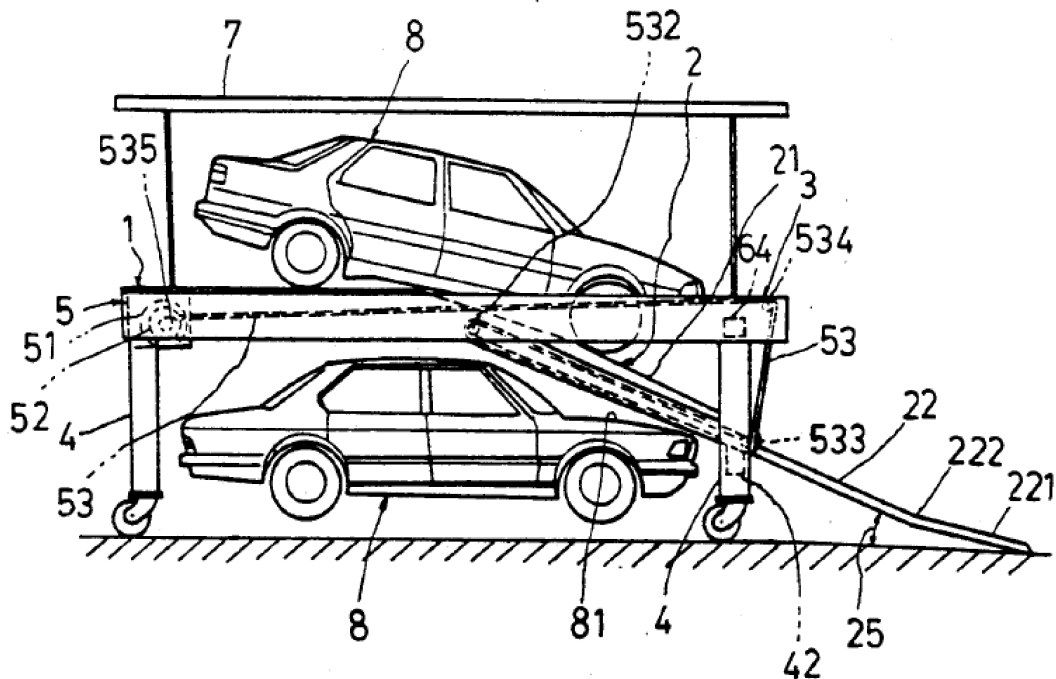


Figure 3 - Patent US 5110250 A

Source: (KUO, 1990).

It is interesting to notice that each vehicle can be parked independently, i.e., it is not necessary to remove one car so that the other can be driven out of the device.

### 3.4 Limit of elastic/plastic behavior

The yield point is the point on a stress–strain curve that indicates the limit of elastic behavior and the beginning of plastic behavior. Prior to the yield point the material will deform elastically and will return to its original shape when the applied stress is removed. Once the yield point is passed, some fraction of the deformation will be permanent and non-reversible.

Figure 4 shows the general stress-strain curve for a steel at room temperature. Yield strength or yield stress is the material property defined as the stress at which a material begins to deform plastically whereas yield point is the point where nonlinear (elastic + plastic) deformation begins (Yield (engineering), 2019).

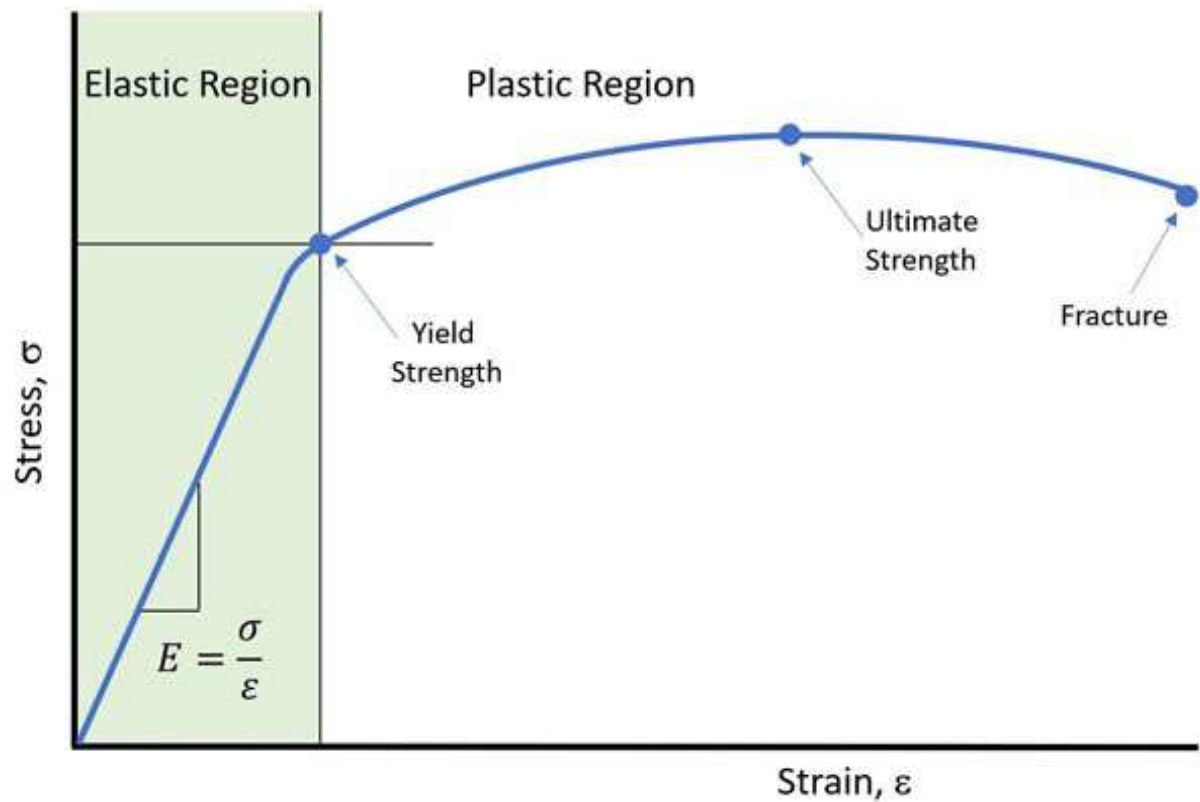


Figure 4 - Stress-strain curve  
Source: (stress-strain-curve).

### 3.5 Dimensioning of machine parts

In the dimensioning of machine parts, the elements to be calculated must bear the loads safely. For this reason, the elements are calculated to present only elastic deformations (not plastic) and therefore the fixed working stress must be less than the yield strength of the material. This stress, which offers the mechanical element a safe working condition, is called permissible stress. The permissible stress is the yield stress divided by a safety factor. Bach's table provides the permissible tensile, compression, bending and torsion stress values for different steels considering three types of loading: static, intermittent and alternating, as shown in Figure 5 (COSTA, 2016).

		Aços									
		ABNT 1010		ABNT 1020		ABNT 1030		ABNT 1040		ABNT 1050	
		Laminado	trefilado	laminado	trefilado	laminado	trefilado	laminado	trefilado	laminado	trefilado
$\sigma_r$		330	370	390	430	480	530	530	600	630	700
$\sigma_e$		180	310	210	360	260	450	290	500	350	590
Along % 10 cm		28	20	25	15	20	12	18	12	15	10
HB		95	105	111	121	137	149	149	170	179	197
Solicitação	Carreg.	Tensão Admissível Segundo Bach (MPa)									
$\sigma_t$	1	80	100	100	140	135	155	150	210	200	220
	2	50	65	65	90	85	100	95	135	125	145
	3	35	45	45	65	60	75	70	90	80	100
$\sigma_c$	1	80	100	100	140	135	155	150	210	200	220
	2	50	65	65	90	85	100	95	135	125	145
	3	35	45	45	65	60	75	70	90	80	100
$\sigma_f$	1	85	110	110	150	145	170	165	230	220	240
	2	55	70	70	100	95	110	105	150	140	160
	3	40	50	50	70	65	80	75	105	95	115
$\tau_t$	1	50	65	65	85	80	100	95	125	115	135
	2	30	40	40	55	50	65	60	80	70	90
	3	20	30	30	40	35	50	45	60	50	70

**LABORATÓRIO DE PROJETOS MECÂNICOS**

1 - Carregamento estático (ex: vigas...)

2 - Carregamento Intermitente (ex: dentes de engrenagens...)

3 - Carregamento Alternado (ex: eixos...)

Figure 5 - Permissible stress according to Bach  
Source: (PERTENCE, 2019).

### 3.6 Shear pin

Shear is a deformation phenomenon to which the body is subjected when the force is applied in the direction perpendicular to its longitudinal axis, causing a displacement in different planes, keeping the volume constant. The shear stress  $\tau_c$  can be calculated as the shear force  $F$  divided by the area  $A$  in which the force is being applied, as it is in the equation below (COSTA, 2016).

$$\tau_c = \frac{F}{A}$$

In the present work, this area is mainly the area of a shaft, which can be calculated with the equation below, where  $d$  is the diameter of the shaft:

$$A = \frac{\pi d^2}{4}$$

Combining the two equations:

$$\tau_c = \frac{F}{A} = \frac{F}{\frac{\pi d^2}{4}} \Rightarrow d = \sqrt{\frac{4F}{\pi \times \tau_c}}$$

If the shear stress  $\tau_c$  is replaced on the equation above by the permissible shear stress of the material, i.e., the maximal shear stress value that secures safe operation, the diameter of the shaft is the minimum diameter that allow the operation without failure or plastic deformation. Thus, the diameter must be bigger than the minimum diameter calculated:

$$d \geq \sqrt{\frac{4F}{\pi \times \tau_c}}$$

### 3.7 Buckling

Members in compression have the potential to buckle: to suddenly lose the ability to carry load by moving laterally with respect to the load. The load which causes a member to buckle depends on the following member properties: the unbraced length  $L$ , the cross section size and "spread-outness"  $I$ , the material stiffness  $E$  and the "effective length factor", denoted by  $k$ . The "effective length factor" represents the end conditions, which are important since they change the effective length of the member, that is why it is accounted for by an "effective length factor", denoted by  $k$  (VIRGINIA, 2010). Figure 6 shows how the effective length factor varies according to the end conditions.

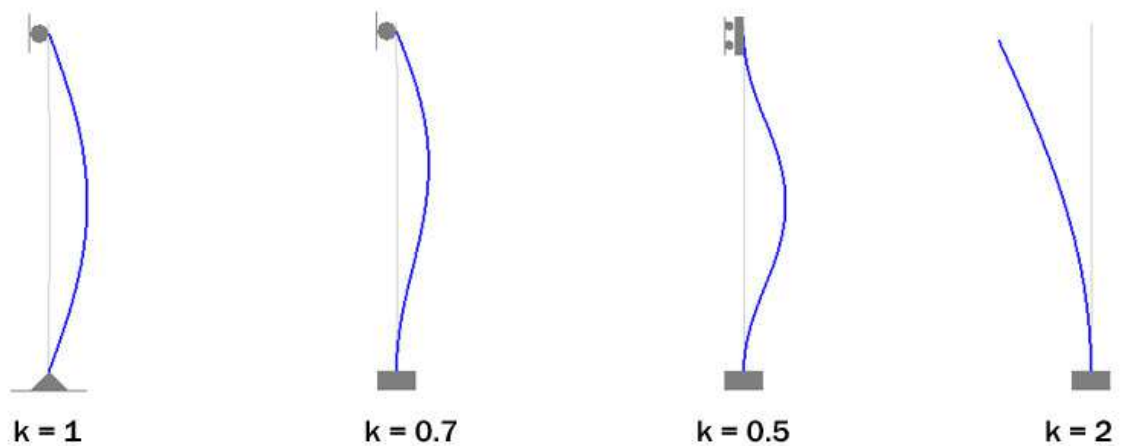


Figure 6 - Effective length factors  
Source: (VIRGINIA, 2010).

The critical buckling stress  $f_{cr}$ , i.e. the maximal value of stress that the material can support, is calculated as above, where  $E$  is the yield strength of the material,  $I$  is the area moment of inertia,  $K$  is the effective length factor,  $L$  is the length and  $A$  is the area.



$$f_{cr} = \frac{\pi^2 E}{\left(\frac{KL}{\sqrt{I/A}}\right)^2}$$

### 3.8 Class 2 lever

A lever is a simple machine consisting of a beam or rigid rod pivoted at a fixed hinge, or fulcrum. A lever amplifies an input force to provide a greater output force, which is said to provide leverage. The ratio of the output force to the input force is the mechanical advantage of the lever. On the basis of the location of fulcrum, load and effort, the lever is divided into three types: class 1, 2 and 3 lever.

Figure 7 shows the class 2 lever. The resistance (or load) is in the middle. The effort is applied on one side of the resistance and the fulcrum is located on the other side, e.g. in a wheelbarrow, a nutcracker, a bottle opener or the brake pedal of a car, the load arm is smaller than the effort arm, and the mechanical advantage is always greater than one. It is also called force multiplier lever. However, in an oar the load arm is greater than the effort arm, and the mechanical advantage is less than one (Lever, 2019).

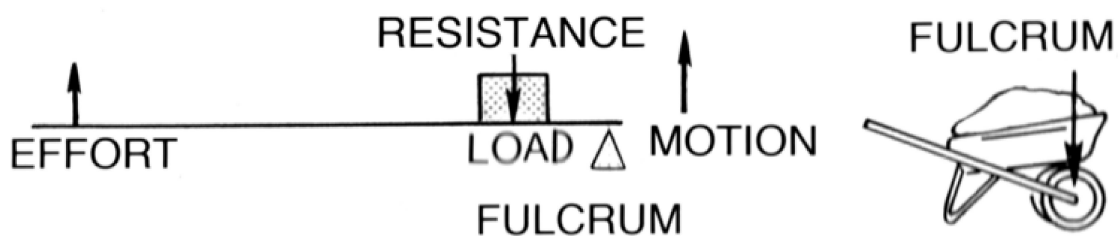


Figure 7 - Class 2 lever  
Source: (Lever, 2019).

### 3.9 Movable pulley

A pulley is a wheel on an axle or shaft that is designed to support movement and change of direction of a taut cable or belt, or transfer of power between the shaft and cable or belt.

The simplest theory of operation for a pulley system assumes that the pulleys and lines are weightless, and that there is no energy loss due to friction. It is also assumed that the lines do not stretch. In equilibrium, the forces on the moving block must sum to zero. In addition the tension in the rope must be the same for each of its parts. This means that the two parts of the rope supporting the moving block must each support half the load.

Figure 8 shows a movable pulley. The load  $F$  on the moving pulley is balanced by the tension in two parts of the rope supporting the pulley. A movable pulley has an axle in a movable block. A single movable pulley is supported by two parts of the same rope and has a mechanical advantage of two (Pulley, 2019).

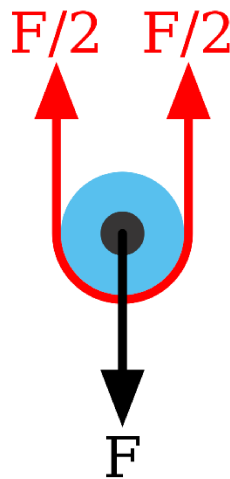


Figure 8 - Movable pulley  
Source: (Pulley, 2019).

### 3.10 Support reactions

The following literature review is taken from (COSTA, 2016).

The determination of the supporting reactions of a body is made by applying the three equilibrium conditions. In order to explain this determination, the reactions  $R_1$  and  $R_2$  of the shaft bearings in Figure 9 will be calculated analytically:

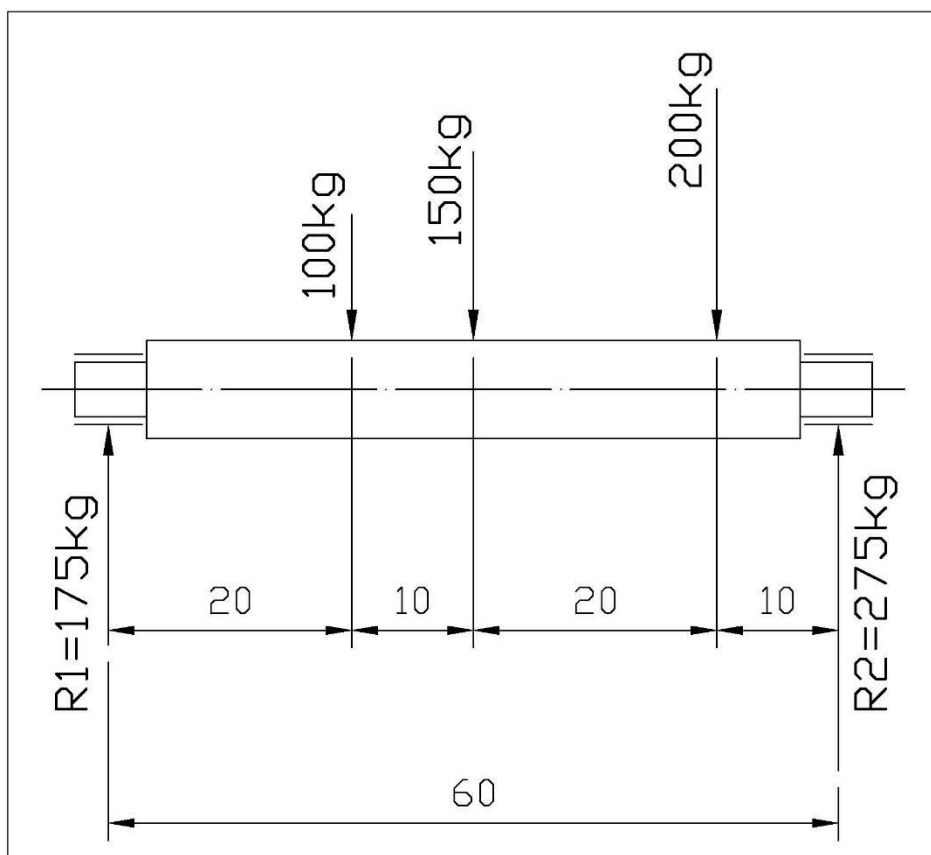


Figure 9 - Shaft with static loading  
Source: (COSTA, 2016).

#### 3.10.1 First condition: $\sum M_i = 0$

It is convenient to calculate the moments in relation to the point where there are the greatest number of unknown forces. In this example, these are the points 1 and 2. Choosing point 1 and counterclockwise as positive results:

$$-100 \times 20 - 150 \times 30 - 200 \times 50 + R_2 \times 60 = 0$$

This equation gives  $R_2$  value:

$$R_2 = \frac{100 \times 20 + 150 \times 30 + 200 \times 50}{60} = 275 \text{ kg}$$

### 3.10.2 Second condition: $\sum V_i = 0$

Convincing upward forces as positive forces, it results:

$$R_1 = 100 + 150 + 200 - 275 = 175 \text{ kg}$$

### 3.10.3 Third condition: $\sum H_i = 0$

This condition is not applied to this problem due to the absence of horizontal forces.

### 3.10.4 Statically indeterminate

According to (wikipedia, 2019), in statics and structural mechanics, a structure is statically indeterminate (or hyperstatic) when the static equilibrium equations (force and moment equilibrium conditions) are insufficient for determining the internal forces and reactions on that structure. To solve statically indeterminate systems (determine the various moment and force reactions within it), one considers the material properties and compatibility in deformations.

## 4 METHODS

The present section comprises the step-by-sept methodology adopted in the development of the device. As the need for free space was perceived in the metropolis around the world, the idea of developing an innovative device capable of parking two vehicles in the same space required to park only one come to mind. So, the device was conceived. In the first step, the basic idea of the device's architectures and its specifications/limitations were defined. A sketch was then designed. Next, from the observation of similar duplicators commercialized, each mechanical component was idealized. A conceptual design was developed in the software SOLIDWORKS® v. 2019. All mechanical components were then dimensioned through analytical and finite element methods. Finally, a virtual prototype was developed in the software SOLIDWORKS® v. 2019. A reduced scale prototype was 3D printed. Simulations and tests took place on both prototypes improving and validating the project. An aid system was developed to assist the driver in the maneuvering to park, avoiding collisions and providing security to the parking duplicator device. Finally a cost estimate was performed, giving an idea of the material necessary to the manufacturing of the equipment and its price. It is important to notice that the steps taken in the development of the device actually happen simultaneously. They do not happen so linearly as it seems, the activities intercept each other.

### 4.1 Design Characteristics and Sketch

This step comprises the discussion of all the characteristics and limitations of the device aiming to design a sketch of the parking duplicator.

From the presented parking problem, a basic idea of the project was proposed for the duplicator and proceeded with obtaining, evaluating, discussing and defining its capabilities, performances and basic characteristics. The dimensions of the parking duplicator were based on the Ford Mustang GT Premium 5.0 2019 and the limitations of the application fields for the device. This vehicle was chosen because of its high weight and dimensions, resulting in a parking device dimensioned to suit virtually any sedan, hatchback or coupe. The device is not dimensioned for SUVs and trucks. Thus, parameters such as the dimensions of the duplicator, the type of drive, the power and the rate of reduction of the gearmotor were idealized, which were used in later stages such as the stress analysis and modeling of the device. This stage also involved the

evaluation and discussion of the basic idea regarding functionality, fabricability (unit or series, spectrum of manufacturing processes), maintenance, durability, economic viability, work safety and environmental viability. The duplicator is intended to be installed primarily in rotary parking companies, apartment buildings, homes and offices. The only requirement for its installation is the ceiling of the building, which must not be lower than 3 m (COSTA, COSTA, *et al.*, 2017).

Once all the above-mentioned characteristics were discussed, a sketch of the device was designed.

## **4.2 Conceptual Design**

According to the sketch and the observation of existing equipment, installations, components and structures that are the same, equivalent or similar to the device under study, all mechanical components necessary for the proper operation of the device were idealized. Thus, a conceptual design was developed for the parking duplicator following the characteristics discussed in the first step. It is through the conceptual design that a solution to the presented problem was in fact conceived. The CAD softwares SOLIDWORKS® v. 2019 and AutoCAD® v. 2016 were used in the execution of the conceptual design (COSTA, COSTA, *et al.*, 2017).

## **4.3 Analytical Dimensioning**

In order to perform the mechanical dimensioning of the duplicator, the components and parts were separated, considering the influence of the efforts of each element on the other and vice versa. Thus the free-body diagrams were obtained, where the efforts can be defined as actions and reactions (COSTA, COSTA, *et al.*, 2017).

It is important to notice that the dimensioning of the mechanical components follows an order. The first component to be dimensioned is the one that does not have efforts from other components of the duplicator been transmitted to it. The first dimensioned component directly receives the load from the elevated vehicle and transmits it to the other components. This order secures that the weight of the dimensioned component can be accordingly computed in the dimensioning of the next element, as once the dimensions of the component is known, it is

possible to calculate its weight which will cause strain on the next element. Thus, the stress analysis of the main components of the duplicator was performed.

Please refer to

APPENDIX A - Drawing 1 where balloons and a table signalize the name of each part of the parking duplicator device.

#### 4.3.1 Folded sheet metal

This section comprises the dimensioning of the sheet metal over which the upper vehicle is parked. It is important to notice that the lift platform is composed by 2 sheet metals, once its architecture is formed of two planes that intercept each other. These sheet metals are important mechanical components of the structure and they must be properly dimensioned securing that the strain causes solely elastic deformation on the material. Figure 10 shows the sheet metals 1 and 2, which will be properly dimensioned on the present section considering the maximal arrow and the maximal bending moment on the sheet metals.

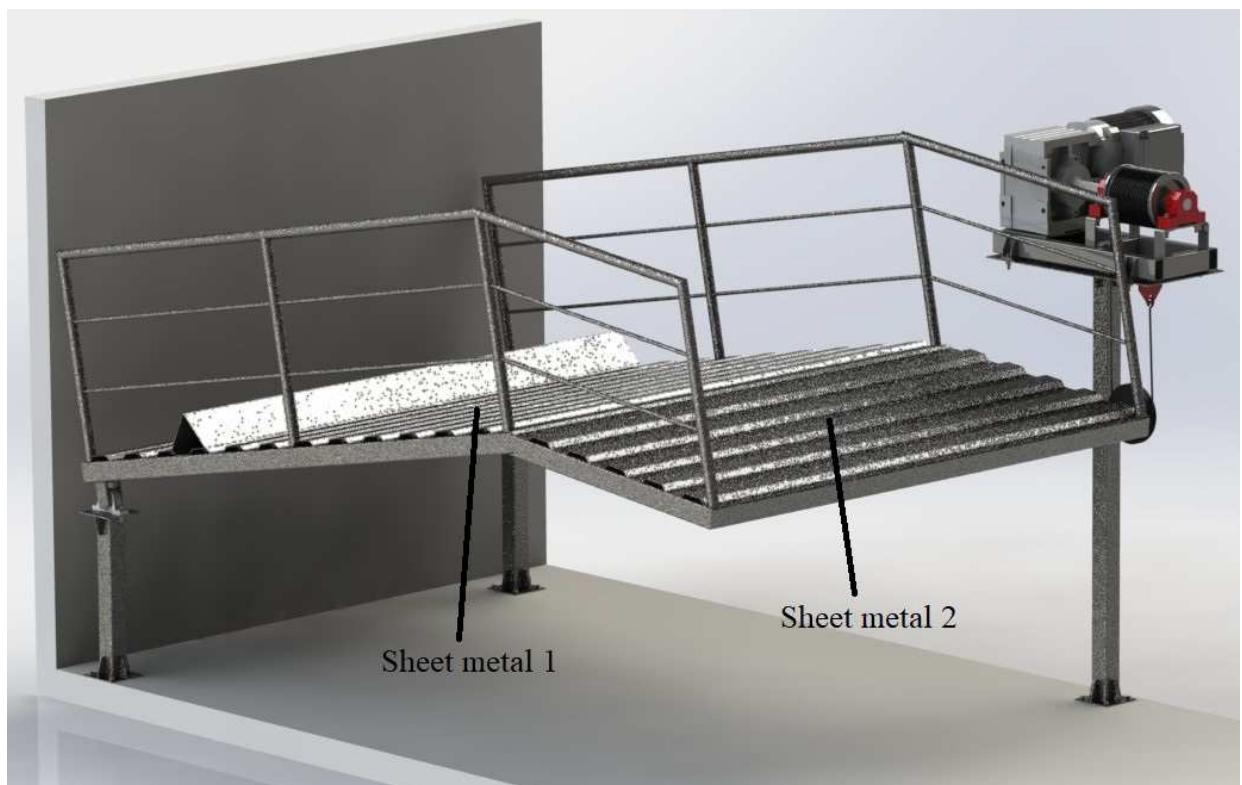


Figure 10 - Sheet metals 1 and 2  
Source: elaborated by the author.

In order to dimension the sheet metals and all the other components of the parking duplicator, the technical specifications of the Ford Mustang GT were considered affording parameters as weight and dimensions of the vehicles. Thus, all mechanical components of the device were dimensioned based on the technical specifications of the Ford Mustang GT Premium 5.0 2019 according to (Ford Mustang 2019, 2019).

The sheets metals support the weight of the elevated vehicle, which is in direct contact with the sheet metals 1 and 2, as shown on Figure 11. The vehicle causes strain on both sheet metals, the dimensioning is made considering that each sheet metal supports half of the strain.

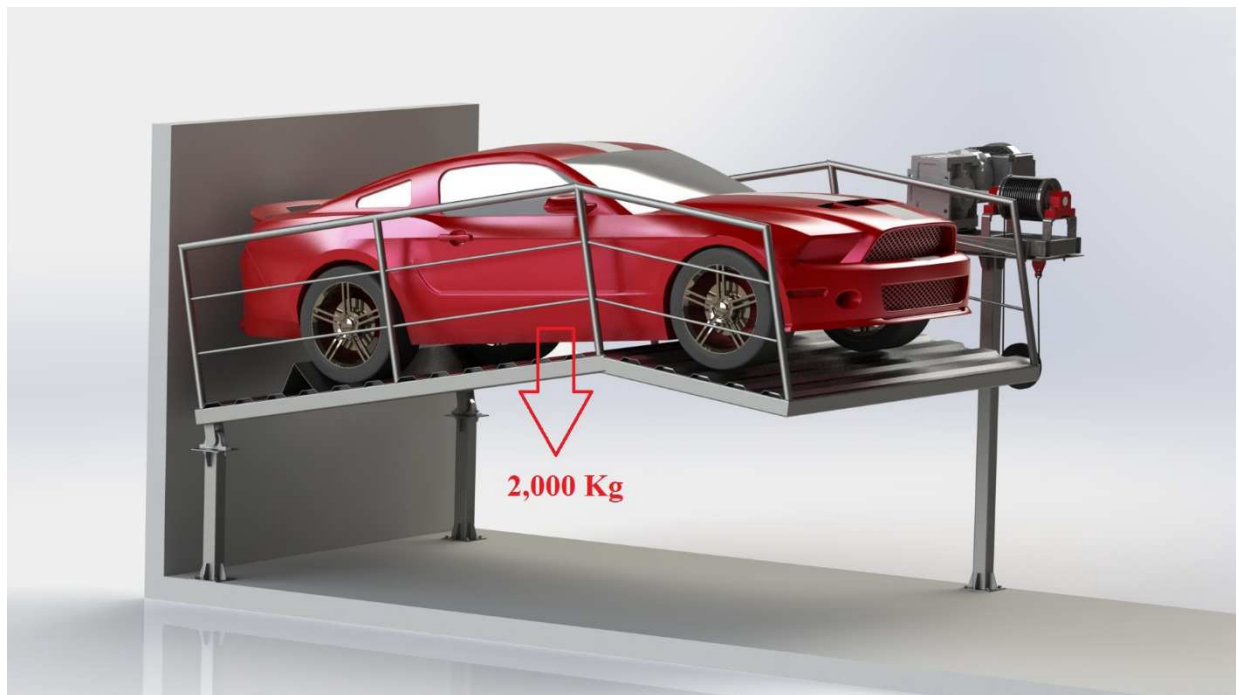


Figure 11 - Strain on the sheet metals  
Source: elaborated by the author.

The load (2,000 kg) over the sheet metals is composed by the weight of the lifted vehicle which is 1,783 kg according to (Ford Mustang 2019, 2019), plus the weight of the driver (adopted 100 kg) and eventual luggage on the trunk, adopted 117 kg.



Load = vehicle + driver + luggage

Load = 1,783 kg + 100 kg + 117 kg = 2,000 kg

Each one of the two sheet metals supports half of the load. Thus, the load distributed on each sheet metal is:

$$\frac{\text{Load}}{2} = 1,000 \text{ kg}$$

Figure 12 shows the architecture of the grid that supports the sheets metals. Figure 13 shows the dimensions of the grid.



Figure 12 - Grid supporting the sheet metals  
Source: (COSTA e VICTORINO, 2019).

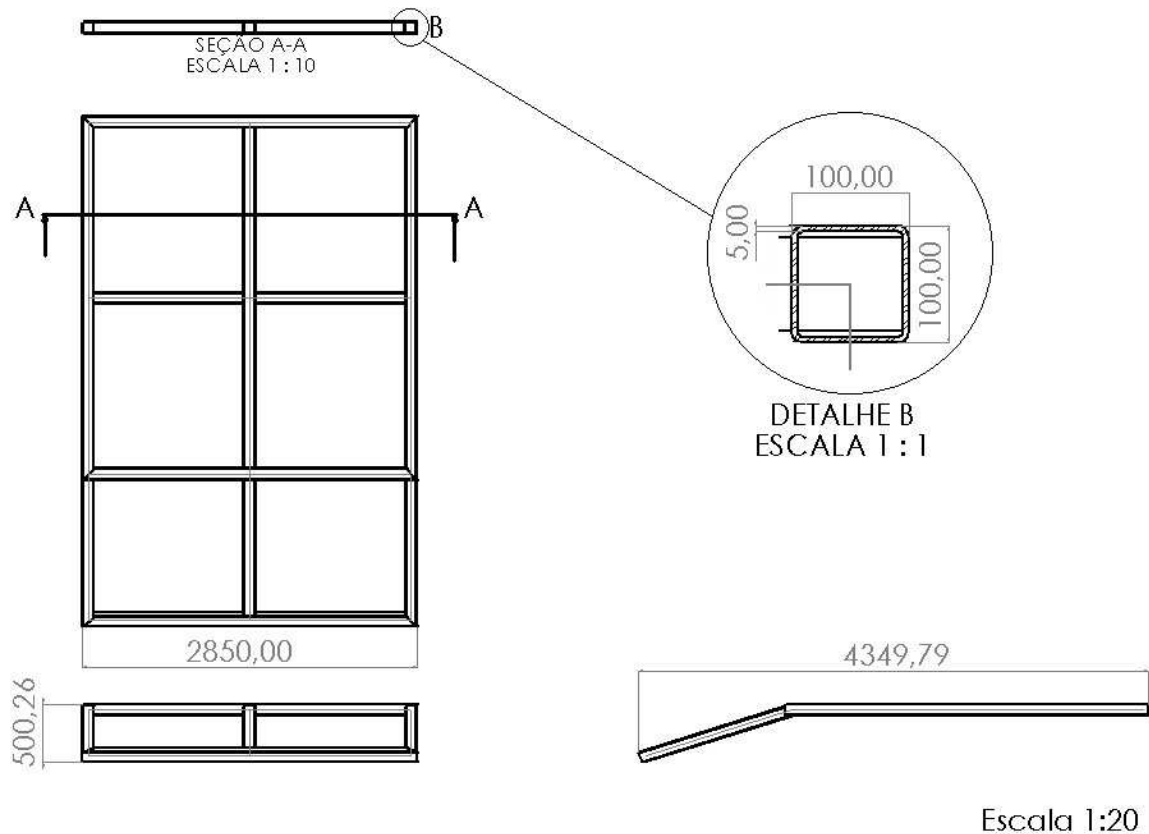


Figure 13 - Dimensions of the grid  
Source: (COSTA e VICTORINO, 2019).

According to Figure 12 and Figure 13, it is possible to realize that the longest free length of the sheet metal which is hanging, or in other words, is not supported, is:

$$L = \frac{2,850 \text{ mm}}{2} = 1425 \text{ mm} = 1.43 \text{ m}$$

The distributed load of the vehicle on the hanging area of the sheet metal can be then calculated as:

$$w_v = \text{Distributed load of the vehicle} = \frac{1,000 \text{ Kg}}{1.43 \text{ m}} = 6,881.86 \frac{\text{N}}{\text{m}}$$

In order to dimension the sheet metals, it is important to consider the weight of the own sheet metals in the dimensioning. Thus considering a sheet metal of 2 mm of thickness, the sheet metal number 1 weighs 145.35 kg and the sheet metal number 2 weighs 66.09 kg - calculated

with SOLIDWORKS® v. 2019. Thus, the distributed load of the sheet metals #1 and #2 can be calculated as:

$$w_{\#1} = \text{Distributed load of sheet metal \#1} = \frac{145.35 \text{ Kg}}{1,43 \text{ m}} = 1.00 \frac{\text{N}}{\text{m}}$$

$$w_{\#2} = \text{Distributed load of sheet metal \#2} = \frac{66.09 \text{ Kg}}{1,43 \text{ m}} = 0.45 \frac{\text{N}}{\text{m}}$$

### **Maximal Arrow**

In order to calculate the maximal arrow on the sheet metals, it is important to know the Elastic modulus ( $E$ ) of the A36 steel which is  $2 \times 10^{11}$  Pa and the moment of inertia in relation to x-axis ( $I_{xx}$ ) for each sheet metal.  $I_{x1}$  for sheet metal #1 is  $840868.47 \text{ mm}^4$  and  $I_{x2}$  for sheet metal #2 is  $369505.04 \text{ mm}^4$  - calculated with SOLIDWORKS® v. 2019.

The maximal arrow on the sheet metal #1 can be calculated as:

$$\delta_{\text{máx1}} = \frac{5 \times (w_v + w_1) \times L^4}{384 \times E \times I_{xx1}} = 2.20 \text{ mm}$$

The maximal arrow on the sheet metal #2 can be calculated as:

$$\delta_{\text{máx2}} = \frac{5 \times (w_v + w_2) \times L^4}{384 \times E \times I_{xx2}} = 5.00 \text{ mm}$$

According to the Eurocode 3, the maximal arrow for the sheet metals is:

$$\delta_{\text{máx}} = \frac{L}{250} = \frac{1425 \text{ mm}}{250} = 5.70 \text{ mm}$$

As the arrows that effectively happen on the structure, i.e.  $\delta_{\text{máx1}}$  and  $\delta_{\text{máx2}}$ , are lower than the maximal arrow suggested by the standard ( $\delta_{\text{máx}}$ ), the sheet metals #1 and #2 with the thickness of 2 mm are both approved for the maximal arrow criteria:

$$\delta_{\text{máx1}} \leq 5.70 \text{ mm} \Rightarrow \text{ok!}$$

$$\delta_{m\acute{a}x2} \leq 5.70 \text{ mm} \Rightarrow \text{ok!}$$

### **Bending Moment**

Once both sheet metals are approved for the maximal arrow criteria, the evaluation of the bending moment is going to be proceeded for the sheet metal of 2 mm. Considering the weight of the sheet metals, the load of the very sheet metal distributed in the thickness is:

$$w_{1t} = \text{Distributed load of sheet metal \#1 on the thickness} = \frac{145.35 \text{ Kg}}{2 \text{ mm}} = 712.72 \frac{\text{N}}{\text{m}}$$

$$w_{2t} = \text{Distributed load of sheet metal \#2 on the thickness} = \frac{66.09 \text{ Kg}}{2 \text{ mm}} = 324.07 \frac{\text{N}}{\text{m}}$$

According to (GRAVINA, 1957), the maximal bending moment is acting at the middle of structure and it can be calculated as:

$$M_{m\acute{a}x} = w \times \cos \alpha \times \frac{a^2}{24}$$

The parameters  $\alpha = 45^\circ$  and  $a = 35.36 \text{ mm}$  have these values because of the architecture of both sheet metals.  $\alpha$  is the inclination angle of the sheet metal segment and  $a$  is its length. The parameters 1.5 and 1.25 multiply the distributed load according to NBR 8800 for security reasons, thus:

$$M_{m\acute{a}x} = (1.5 \times w_v + 1.25 \times w_{1t}) \times \cos \alpha \times \frac{a^2}{24}$$

Replacing the values for each one of the sheet metals:

$$M_{m\acute{a}x1} = \left( 1.5 \times 6,881.86 \frac{\text{N}}{\text{m}} + 1.25 \times 712.72 \frac{\text{N}}{\text{m}} \right) \times \cos 45^\circ \times \frac{0.04^2}{24} = 0.41 \text{ Nm}$$

$$M_{m\acute{a}x2} = \left( 1.5 \times 6,881.86 \frac{\text{N}}{\text{m}} + 1.25 \times 324.07 \frac{\text{N}}{\text{m}} \right) \times \cos 45^\circ \times \frac{0.04^2}{24} = 0.40 \text{ Nm}$$

The maximal bending moment acting on the sheet metal is  $M_{m\acute{a}x1} = 0.41 Nm$  for the sheet metal #1 and  $M_{m\acute{a}x2} = 0.40 Nm$  for the sheet metal #2.

The permissible bending moment for the A36 steel according to BACH table is  $12.25 \frac{kg}{mm^2}$  for the presented load condition (PROVENZA, 1990).

The resistance module for the problem ( $W_x$ ) is calculated as the maximal bending moment acting on the sheet metal divided per the permissible bending moment of the material. The permissible bending moment of the material was taken from (PROVENZA, 1990) considering the ABNT 1045 steel.

$$W_{x1} = \frac{0.41 Nm}{12,250 \frac{kg}{mm^2}} = 33.72 mm^3$$

$$W_{x2} = \frac{0.40 Nm}{12.25 \frac{kg}{mm^2}} = 32.26 mm^3$$

The resistance module for the problem must be lower then the resistance module of the profile, which is the maximal value of the resistance module that the profile can support. The resistance module of the profile ( $W$ ) is calculated as the moment of inertia in relation to x-axis ( $I_{xx}$ ) divided per the heath of the distance between the center of mass and the most distant fiber of the structure ( $h$ ):

$$W = \frac{I_{xx}}{\frac{h}{2}}$$

The resistance module of the profile ( $W$ ) for each sheet metal is:

$$W_1 = \frac{I_{xx1}}{\frac{h}{2}} = 41,148.44 mm^3$$

$$W_2 = \frac{I_{xx2}}{\frac{h}{2}} = 18,081.97 mm^3$$

As it can be seen, the resistance module for the problem is lower than the resistance module of the profile:

$$W_{x1} = 33.72 \text{ mm}^3 \leq w_1 = 41,148.44 \text{ mm}^3 \Rightarrow \text{ok!}$$

$$W_{x2} = 32.26 \text{ mm}^3 \leq w_2 = 18,081.97 \text{ mm}^3 \Rightarrow \text{ok!}$$

Thus, the sheet metals #1 and #2 are approved with the thickness of 2 mm. There will occur only elastic deformation on the structure. There will not be plastic deformation, thus the structure will work securely with the presented load condition.

#### 4.3.2 Grid

The stress-strain analysis was performed in order to determine the minimum thickness of the rectangular structural profile that constitutes the grid. The load was calculated as transmitted from the elevated vehicle to the folded sheet metal over which the upper vehicle is parked and so, finally transmitted to the grid as an uniformly distributed load. The load condition primarily subjects the grid to a shear stress, twisting and bending moments. The grid will then be dimensioned to resist to these 3 types of solicitations. The strain acting on the grid was calculated in the structural analysis software MASTAN2® as shown in Figure 14, which displays the shear force on the grid.

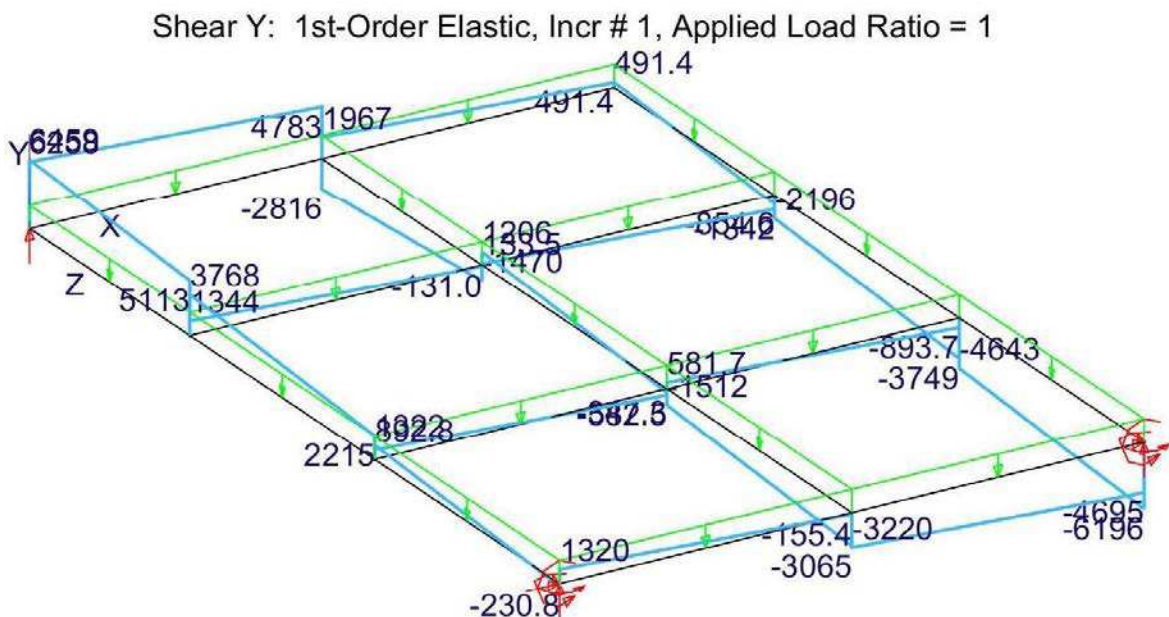


Figure 14 - Grid structural analysis in the software MASTAN2® exhibiting the bending moment  
Source: (COSTA, 2017).

### Shear Stress

First the grid will be dimensioned to the shear stress. The maximal shear force acting on the grid is 6,459 N. This value was calculated in the software MASTAN2® and it includes the load of the lifted vehicle, the sheet metals and the own grid's weight, assuming a grid with a rectangular profile with a thickness of 5 mm. If this profile is approved in the present dimensioning, it will be the selected profile for the construction of the grid.

The area of the section of this rectangular profile with 5 mm thickness is 18.20 cm<sup>2</sup> and it was calculated with the software SOLIDWORKS® v. 2019.

The maximal shear stress ( $\tau_{m\acute{a}x}$ ) acting on the grid is the shear force divided by the cross-section area of the rectangular profile, thus:

$$\tau_{m\acute{a}x} = \frac{6,459 \text{ N}}{18.20 \text{ cm}^2} = 3.55 \frac{\text{N}}{\text{mm}^2}$$

The permissible shear stress for the A36 steel according to BACH table is  $6.50 \frac{\text{kg}}{\text{mm}^2}$  ( $63.74 \frac{\text{N}}{\text{mm}^2}$ ) for the presented load condition (PROVENZA, 1990). The maximal shear stress ( $\tau_{m\acute{a}x}$ ) acting on the grid must be lower than the permissible shear stress for the A36 steel, which is the maximal value of shear stress that the material can support at this load condition. As this requisite is accomplished, the grid with the rectangular profile of 5 mm thickness is properly dimensioned for the shear stress:

$$\tau_{m\acute{a}x} = 3.55 \frac{\text{N}}{\text{mm}^2} \leq 63.74 \frac{\text{N}}{\text{mm}^2} \Rightarrow \text{ok!}$$

## **Bending Moment**

Second, the grid will be dimensioned to the bending moment. The resistance module of the problem can be calculated as:

The maximal bending moment acting on the grid was calculated with the software MASTAN2® and its value is  $M_{m\acute{a}x} = 6,175 \text{ Nm}$ .

The resistance module for the problem ( $W_x$ ) is calculated as the maximal bending moment acting on the sheet metal divided per the permissible bending moment of the material. The permissible bending moment of the material was taken from the BACH table at (PROVENZA, 1990) considering the ABNT 1045 steel and is  $12.25 \frac{kg}{mm^2}$  for the presented load condition.

$$W_x = \frac{6,175 \text{ Nm}}{12.25 \frac{kg}{mm^2}} = 51.40 \text{ cm}^3$$

The resistance module for the problem must be lower then the resistance module of the profile, which is the maximal value of the resistance module that the profile can support. The resistance module of the profile ( $W$ ) is afforded by the supplier's catalog (Tubos Estruturais: Seção Circular, Quadrada e Retangular, 2019) and is  $W = 54.20 \text{ cm}^3$ .

As it can be seen, the resistance module for the problem is lower then the resistance module of the profile:

$$W_x = 51.40 \text{ cm}^3 \leq W = 54.20 \text{ cm}^3 \Rightarrow \text{ok!}$$

Thus, the grid with the thickness of 5 mm is approved for the bending moment criteria. There will occur only elastic deformation on the structure. There will not be plastic deformation, thus the structure will work securely with the presented load condition.



## Torsion

Third, the grid will be dimensioned for the torsion. The maximal twisting moment occurring on the grid is 3,208 Nm – calculated with the software MASTAN2®.

The resistance module to torsion for the problem ( $W_t$ ) is calculated as the maximal twisting moment acting on the sheet metal divided per the permissible twisting moment of the material. The permissible twisting moment of the material was taken from the BACH table at (PROVENZA, 1990) considering the ABNT 1045 steel and is  $6.50 \frac{kg}{mm^2}$  for the presented load condition.

$$W_t = \frac{3,208 \text{ Nm}}{6.50 \frac{kg}{mm^2}} = 50.33 \text{ cm}^3$$

The resistance module to torsion for the problem must be lower then the resistance module to torsion of the profile, which is the maximal value of the resistance module to torsion that the profile can support. The resistance module to torsion of the profile ( $W$ ) is afforded by the supplier's catalog (Tubos Estruturais: Seção Circular, Quadrada e Retangular, 2019) and is  $W = 81.70 \text{ cm}^3$ .

As it can be seen, the resistance module to torsion for the problem is lower then the resistance module to torsion of the profile:

$$W_x = 50.33 \text{ cm}^3 \leq W = 81.70 \text{ cm}^3 \Rightarrow \text{ok!}$$

Thus, the grid with the thickness of 5 mm is approved for the twisting moment criteria. There will occur only elastic deformation on the structure. There will not be plastic deformation, thus the structure will work securely with the presented load condition.

## **Considerations**

The designed grid has shown to be relatively well resistant to the shear stress and the twisting moment. The bending moment is the limiting strain acting on it. Once the grid is dimensioned to resist the bending moment, the conditions required by the shear stress and the torsion moment are simultaneously attended.

The thickness of the rectangular profile of the beams that form the grid is chosen according to the resistance modulus of the profile, which is selected to guarantee that the structural element won't suffer plastic deformation. If the selected beam has a resistance module higher than the one calculated for the problem, there will only be elastic deformations and the mechanical component won't fail. (COSTA, COSTA, *et al.*, 2017).

Thus the profile selected for the grid is rectangular as has a thickness of 5 mm.

### 4.3.2 Pivots

The pivots are the two pillars supporting the lift platform, where the bearing articulate the lift platform. The pivots are dimensioned for compression, buckling, bending moment, shear stress and maximal arrow.

## **Compression**

The load causing the compression on the pivots is composed by the weight of the lifted vehicle, sheet metals and grid. The weight of the vehicle (plus driver, luggage) is 2,000 as aforementioned. Sheet metal #1 weights 145.36 kg and sheet metal #2 weights 72.68 kg – calculated with SOLIDWORKS® v. 2019 for the selected sheet metals with 2 mm thickness. The weight of the grid is 347.49 kg – calculated with SOLIDWORKS® v. 2019 for the selected rectangular profile with 5 mm thickness. Figure 15 shows the load on the pivots. Where the load  $Q = 2,000 \text{ kg} + 145.36 \text{ kg} + 72.68 \text{ kg} + 347.49 \text{ kg} = 2565.52 \text{ kg}$ .

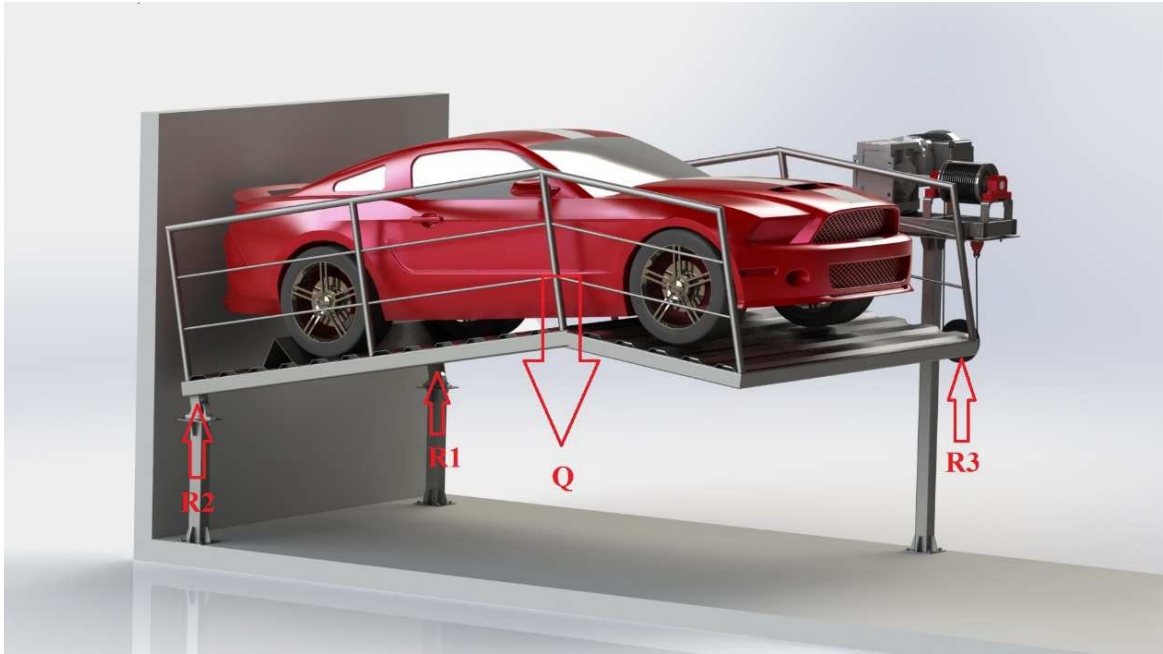


Figure 15 - Load on the Pivots and Pillars  
Source: elaborated by the author.

The reactions  $R_1$ ,  $R_2$  and  $R_3$  can be calculated with the sum of the momentums as below, considering that the length of the platform is  $2d$ :

$$+Qd - 2R_3d = 0$$

$$2R_3d = Qd$$

$$2R_3 = Q$$

$$R_3 = \frac{Q}{2}$$

Thus, replacing this result in the equation of the sum of the y-axis forces:

$$Q = R_1 + R_2 + R_3$$

$$Q = R_1 + R_2 + \frac{Q}{2}$$

$$R_1 + R_2 = \frac{P}{2}$$

It is known that  $R_1 = R_2$ , thus:

$$R_1 = R_2 = \frac{Q}{4}$$

As above calculated, the load on each pivot is one quarter of the load on the lift platform. For security reasons, the loads on the lift platform will be multiplied by the parameters 1.5 and 1.25 according to NBR 8800 as follows:

$$\text{compression load} = \frac{1.5 \times 2,000 \text{ kg} + 1.25 \times (145.36 \text{ kg} + 72.68 \text{ kg} + 347.49 \text{ kg})}{4}$$

$$\text{compression load} = 926.73 \text{ kg} = 9088.08 \text{ N}$$

The architecture of the pivot is a rectangular profile with 5 mm thickness. If these calculations secure a safe condition of operation with this architecture, it will be selected. The cross-section area  $A$  of the pivots was calculated with SOLIDWORKS® v. 2019:

$$A = 18.20 \text{ cm}^2$$

The compression stress acting on each one of the two pivots is named the work compression stress  $\sigma_{work}$ . It can be calculated as:

$$\sigma_{work} = \frac{\text{compression load}}{A} = \frac{9088.08 \text{ N}}{18.20 \text{ cm}^2} = 4.99 \text{ MPa}$$

The permissible compression stress for the A36 steel according to BACH table is  $11 \frac{\text{kg}}{\text{mm}^2}$  (107.87 MPa) for the presented load condition (PROVENZA, 1990). The compression stress ( $\sigma_{work}$ ) acting on the pivot must be lower than the permissible compression stress for the A36 steel, which is the maximal value of compression stress that the material can support at this load condition. As this requisite is accomplished, the pivot with the rectangular profile with 5 mm thickness is properly dimensioned for the compression stress:

$$\sigma_{work} = 4.99 \text{ MPa} \leq 107.87 \text{ MPa} \Rightarrow \text{ok!}$$

Another consideration relatively to the compression deals with the yield strength  $E$ , which must be higher than the compression stress acting on the pivot ( $\sigma_{work}$ ). For the A36 steel,  $E = 250$  MPa according to (A36 steel, 2019). Thus:

$$E = 250 \text{ MPa} \geq \sigma_{work} = 4.99 \text{ MPa} \Rightarrow \text{ok!}$$

### **Buckling**

The buckling on the pivots was evaluated according to (VIRGINIA, 2010). Thus, the critical buckling stress  $f_{cr}$  is calculated as above, where the  $E$  is the yield strength of the A36 steel,  $I$  is the area moment of inertia,  $K$  is the effective length factor,  $L$  is the length and  $A$  is the area of the pivot. According to (VIRGINIA, 2010),  $K = 2$ . According to (A36 steel, 2019),  $E = 250$  MPa. As calculated with SOLIDWORKS® v. 2019,  $L = 0.8$  m,  $A = 18.20 \text{ cm}^2$  and  $I = 271 \text{ cm}^4$ .

$$f_{cr} = \frac{\pi^2 E}{\left(\frac{KL}{\sqrt{I}}\right)^2} = \frac{\pi^2 \times 250 \text{ MPa}}{\left(\frac{2 \times 0.8 \text{ m}}{\sqrt{\frac{271 \text{ cm}^4}{18.20 \text{ cm}^2}}}\right)^2} = 2296.24 \text{ MPa}$$

The compression stress acting on the pivot ( $\sigma_{work}$ ) must be lower than the critical stress ( $f_{cr}$ ). As this requisite is accomplished, the pivot with the rectangular profile with 5 mm thickness is properly dimensioned for the buckling:

$$\sigma_{work} = 4.99 \text{ MPa} \leq f_{cr} = 2296.24 \text{ MPa} \Rightarrow \text{ok!}$$

## Bending Moment

The main solicitations to the pivots are the compression and the buckling. The bending moment happens when the vehicle is driven up onto the lift platform, causing a force that will originate bending moment on the pivots.

In order to calculate this force, consider a vehicle moving at  $V_0 = 1 \frac{m}{s}$ , this vehicle is driving in a straight line at the parking lot as shown on Figure 16, its trajectory is in reverse gear from the ground onto the lift platform, where the vehicle will be parked in order to be lifted in the parking duplicator device. Thus its final velocity  $V_f = 0 \frac{m}{s}$ . It is going to be considered that the vehicle drives a distance  $d = 4.30 m$  in this straight maneuver in reverse gear until it is parked on the lift platform.



Figure 16 - Parking maneuver onto the platform  
Source: elaborated by the author.

Considering that the acceleration is constant and neglecting wind resistance and friction, the acceleration  $a$  of the vehicle can be calculated with the Torricelli's equation as follows:

$$a = \frac{V_f^2 - V_0^2}{2d} = \frac{(0 \frac{m}{s})^2 - (1 \frac{m}{s})^2}{2 \times 4.30 m} = -0.12 \frac{m}{s^2}$$

The force responsible for the deceleration of the vehicle can be calculated with Newton's second law of motion, where  $m = 2,000 \text{ kg}$  is the mass of the vehicle:

$$F = ma = 2,000 \text{ kg} \times \left(-0.12 \frac{\text{m}}{\text{s}^2}\right) = -232.56 \text{ N}$$

This force  $F$  causes the bending moment on the tow pivots. Thus, half of the force acts on each one of the pivots. The maximal bending moment acting on the pivot can be then calculated as follows, where  $L = 0.8 \text{ m}$  is the length of the pivot:

$$M_{max} = \frac{F}{2} \times L = \frac{-232.56 \text{ N}}{2} \times 0.8 \text{ m} = -93.02 \text{ Nm}$$

The resistance module for the problem ( $W_x$ ) is calculated as the maximal bending moment acting on the sheet metal divided per the permissible bending moment of the material. The permissible bending moment of the material was taken from the BACH table at (PROVENZA, 1990) considering the ABNT 1045 steel and is  $12.25 \frac{\text{kg}}{\text{mm}^2}$  for the presented load condition.

$$W_x = \frac{93.02 \text{ Nm}}{12.25 \frac{\text{kg}}{\text{mm}^2}} = 0.77 \text{ cm}^3$$

The resistance module for the problem must be lower than the resistance module of the profile, which is the maximal value of the resistance module that the profile can support. The resistance module of the profile ( $W$ ) is afforded by the supplier's catalog (Tubos Estruturais: Seção Circular, Quadrada e Retangular, 2019) and is  $W = 59.20 \text{ cm}^3$ .

As it can be seen, the resistance module for the problem is lower than the resistance module of the profile:

$$W_x = 0.77 \text{ cm}^3 \leq W = 59.20 \text{ cm}^3 \Rightarrow \text{ok!}$$

Thus, the pivot with the rectangular profile with 5 mm thickness is approved for the bending moment criteria. There will occur only elastic deformation on the structure. There will not be plastic deformation, thus the structure will work securely with the presented load condition.

## Shear Stress

The maximal shear stress ( $\tau_{m\acute{a}x}$ ) on the pivot is calculated as the horizontal force caused by the vehicle's parking maneuver divided for the shear area (A), i.e., the cross-section area of the pivot.

$$\tau_{m\acute{a}x} = \frac{\frac{F}{2}}{A} = \frac{\frac{232.56 \text{ N}}{2}}{18.20 \text{ cm}^2} = 0.06 \frac{\text{N}}{\text{mm}^2}$$

The permissible shear stress for the A36 steel according to BACH table is  $6.50 \frac{\text{kg}}{\text{mm}^2}$  ( $63.74 \frac{\text{N}}{\text{mm}^2}$ ) for the presented load condition (PROVENZA, 1990). The maximal shear stress ( $\tau_{m\acute{a}x}$ ) acting on the pivot must be lower than the permissible shear stress for the A36 steel, which is the maximal value of shear stress that the material can support at this load condition. As this requisite is accomplished, the pivot with the rectangular profile of 5 mm thickness is properly dimensioned for the shear stress:

$$\tau_{m\acute{a}x} = 0.06 \frac{\text{N}}{\text{mm}^2} \leq 63.74 \frac{\text{N}}{\text{mm}^2} \Rightarrow \text{ok!}$$

## Maximal Arrow

In order to calculate the maximal arrow on the pivots, it is important to know the Elastic modulus ( $E$ ) of the A36 steel which is  $2 \times 10^{11}$  Pa and the moment of inertia in relation to x-axis ( $I_{xx}$ ) for the pivot.  $I_{xx} = 271 \text{ cm}^4$  - calculated with SOLIDWORKS® v. 2019.

The arrow acting on the pivot can be calculated as:

$$\delta = \frac{\frac{F}{2} \times L^3}{3 \times (E \times I_{xx})} = \frac{\frac{232.56 \text{ N}}{2} \times (0.8 \text{ m})^3}{3 \times (2 \times 10^{11} \times 271 \text{ cm}^4)} = 0.04 \text{ mm}$$

According to the Eurocode 3, the maximal arrow for the pivot is:

$$\delta_{m\acute{a}x} = \frac{L}{250} = \frac{0.8 \text{ m}}{250} = 3.20 \text{ mm}$$



As the arrow that effectively happens on the structure, i.e.  $\delta$ , is lower than the maximal arrow suggested by the standard ( $\delta_{max}$ ), the pivot with the rectangular profile with 5 mm thickness is approved for the maximal arrow criteria:

$$\delta = 0.04 \text{ mm} \leq \delta_{max} = 3.20 \text{ mm} \Rightarrow \text{ok!}$$

### 4.3.3 Pillar

The pillar is the third structure supporting the lift platform, where the movable pulley lifts the elevating platform. The pillar is dimensioned for compression and buckling.

#### **Compression**

The load causing the compression on the pillar is composed by the weight of the lifted vehicle, sheet metals and grid. The weight of the vehicle (plus driver, luggage) is 2,000 as aforementioned. Sheet metal #1 weights 145.36 kg and sheet metal #2 weights 72.68 kg – calculated with SOLIDWORKS® v. 2019 for the selected sheet metals with 2 mm thickness. The weight of the grid is 347.49 kg – calculated with SOLIDWORKS® v. 2019 for the selected rectangular profile with 5 mm thickness. Figure 15 shows the load on the pillar. Where the load  $Q = 2,000 \text{ kg} + 145.36 \text{ kg} + 72.68 \text{ kg} + 347.49 \text{ kg} = 2565.52 \text{ kg}$ .

The reactions  $R_1$ ,  $R_2$  and  $R_3$  can be calculated with the sum of the momentums as below, considering that the length of the platform is  $2d$ :

$$+Qd - 2R_3d = 0$$

$$2R_3d = Qd$$

$$2R_3 = Q$$

$$R_3 = \frac{Q}{2}$$

As above calculated, the load on the pillar is half of the load on the lift platform. For security reasons, the loads on the lift platform will be multiplied by the parameters 1.5 and 1.25 according to NBR 8800 as follows. For the pillar, the weight of the gearmotor (considered 50 kg) will be added to the compression load once the pillar is supporting the gearmotor's weight as well.

$$\text{compression load} = \frac{1.5 \times 2,000 \text{ kg} + 1.25 \times (145.36 \text{ kg} + 72.68 \text{ kg} + 347.49 \text{ kg})}{2} + 50 \text{ kg} = 1903.45 \text{ kg}$$

$$\text{compression load} = 18,666.48 \text{ N}$$

The architecture of the pillar is a rectangular profile with 5 mm thickness. If these calculations secure a safe condition of operation with this architecture, it will be selected. The cross-section area  $A$  of the pivots was calculated with SOLIDWORKS® v. 2019:

$$A = 18.20 \text{ cm}^2$$

The compression stress acting on the pillar is named the work compression stress  $\sigma_{work}$ . It can be calculated as:

$$\sigma_{work} = \frac{\text{compression load}}{A} = \frac{18,666.48 \text{ N}}{18.20 \text{ cm}^2} = 10.26 \text{ MPa}$$

The permissible compression stress for the A36 steel according to BACH table is  $11 \frac{\text{kg}}{\text{mm}^2}$  (107.87 MPa) for the presented load condition (PROVENZA, 1990). The compression stress ( $\sigma_{work}$ ) acting on the pillar must be lower than the permissible compression stress for the A36 steel, which is the maximal value of compression stress that the material can support at this load condition. As this requisite is accomplished, the pillar with the rectangular profile with 5 mm thickness is properly dimensioned for the compression stress:

$$\sigma_{work} = 10.26 \text{ MPa} \leq 107.87 \text{ MPa} \Rightarrow \text{ok!}$$

Another consideration relatively to the compression deals with the yield strength  $E$ , which must be higher than the compression stress acting on the pillar ( $\sigma_{work}$ ). For the A36 steel,  $E = 250$  MPa according to (A36 steel, 2019). Thus:

$$E = 250 \text{ MPa} \geq \sigma_{work} = 10.26 \text{ MPa} \Rightarrow \text{ok!}$$

### **Buckling**

The buckling on the pillar was evaluated according to (VIRGINIA, 2010). Thus, the critical buckling stress  $f_{cr}$  is calculated as above, where the  $E$  is the yield strength of the A36 steel,  $I$  is the area moment of inertia,  $K$  is the effective length factor,  $L$  is the length and  $A$  is the area of the pillar. According to (VIRGINIA, 2010),  $K = 2$ . According to (A36 steel, 2019),  $E = 250$  MPa. As calculated with SOLIDWORKS® v. 2019,  $L = 2.10$  m,  $A = 18.20 \text{ cm}^2$  and  $I = 220.50 \text{ cm}^4$ .

$$f_{cr} = \frac{\pi^2 E}{\left(\frac{KL}{\sqrt{I}}\right)^2} = \frac{\pi^2 \times 250 \text{ MPa}}{\left(\frac{2 \times 2.10 \text{ m}}{\sqrt{\frac{220.50 \text{ cm}^4}{18.20 \text{ cm}^2}}}\right)^2} = 271.14 \text{ MPa}$$

The compression stress acting on the pillar ( $\sigma_{work}$ ) must be lower than the critical stress ( $f_{cr}$ ). As this requisite is accomplished, the pillar with the rectangular profile with 5 mm thickness is properly dimensioned for the buckling:

$$\sigma_{work} = 10.26 \text{ MPa} \leq f_{cr} = 271.14 \text{ MPa} \Rightarrow \text{ok!}$$

#### 4.3.4 Gearmotor

In order to select the gearmotor, it is necessary to calculate, among other values, the power necessary to elevate the vehicle. The present section comprises all the calculus for the selection of the gearmotor.

Figure 17 shows how the parking duplicator device works as a second-class lever, where the resistance load is between the fulcrum and the effort.

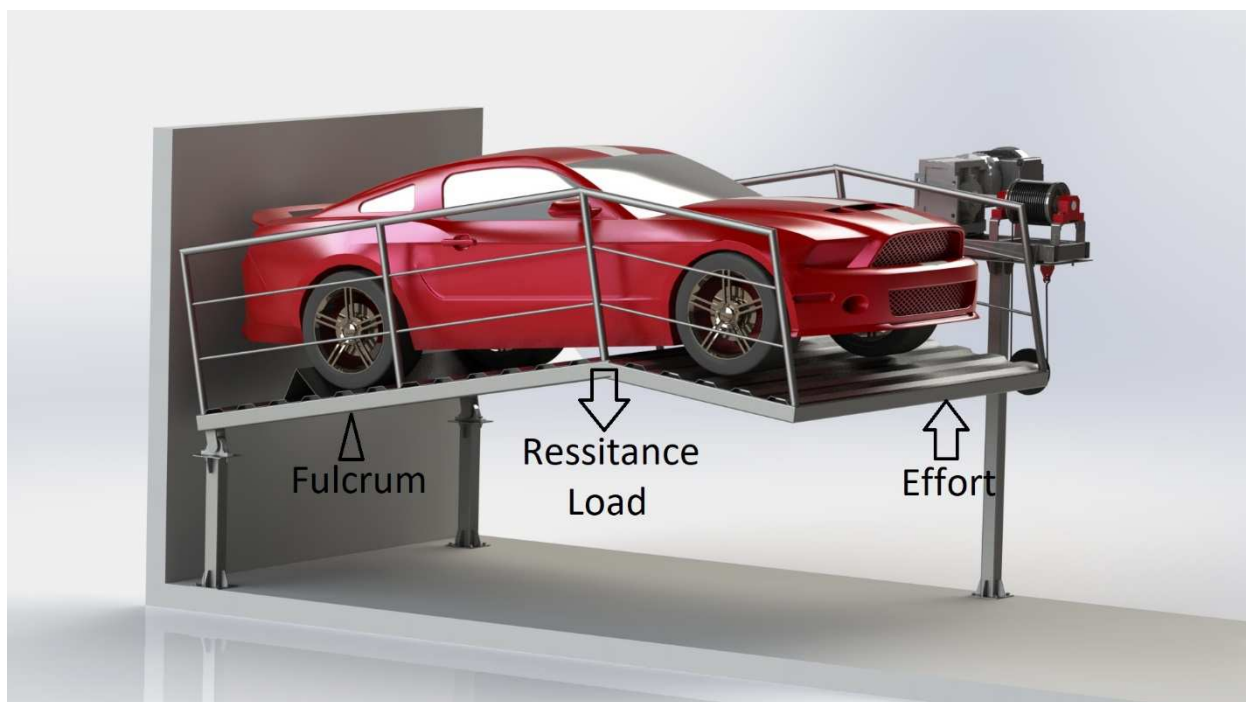


Figure 17 - Parking duplicator device as a second-class lever  
Source: elaborated by the author.

The effort ( $F$ ) to elevate the vehicle can be then calculated by doing the sum of the momentums in relation to the fulcrum, considering that the length of the platform is  $2d$  and that the resistance load ( $Q$ ) is applied at the middle of the platform:

$$F \times 2d - Q \times d = 0$$

$$2Fd = Qd$$

$$2F = Q$$

$$F = \frac{Q}{2}$$

The effort is composed by the weight of the lifted vehicle, sheet metals and grid. The weight of the vehicle (plus driver, luggage) is 2,000 as aforementioned. Sheet metal #1 weights 145.36 kg and sheet metal #2 weights 72.68 kg – calculated with SOLIDWORKS® v. 2019 for the selected sheet metals with 2 mm thickness. The weight of the grid is 347.49 kg – calculated with SOLIDWORKS® v. 2019 for the selected rectangular profile with 5 mm thickness. Thus, the load  $Q = 2,000 \text{ kg} + 145.36 \text{ kg} + 72.68 \text{ kg} + 347.49 \text{ kg} = 2565.52 \text{ kg}$  and  $F$  is:

$$F = \frac{2565.52 \text{ kg}}{2} = 1282.76 \text{ kg} = 12,579.58 \text{ N}$$

The power  $P$  can be calculated with the equation below, where  $v$  is the velocity of the lift platform and  $F_0 = \frac{12,579.58 \text{ N}}{2} = 6,289.79 \text{ N}$  is the force that the gearmotor must do in order to elevate the vehicle.  $F_0$  is  $F$  divided by 2 because there is one movable pulley on the parking device.

$$P = \frac{6,289.79 \text{ N} \times v}{60} = \frac{6,289.79 \text{ N} \times 2 \frac{\text{m}}{\text{min}}}{60} = 0.21 \text{ kW}$$

Considering an efficiency  $\rho = 85 \%$ , the effective power of the gearmotor can be calculated as:

$$P_{ef} = \frac{P}{\rho} = \frac{0.22 \text{ kW}}{0.85} = 0.25 \text{ kW} = 0.34 \text{ cv}$$

The rotation speed of the gearmotor's drum ( $v_f$ ) is two times the speed of the lift platform, because there is one movable pulley. Thus:

$$v_f = 2v = 2(2 \frac{\text{m}}{\text{min}}) = 4 \frac{\text{m}}{\text{min}}$$

The rotation speed  $n$  of the gearmotor can be calculated with the equation below, where  $v_f$  is the speed of the gearmotor's drum and the diameter of the gearmotor's drum is considered to be  $D = 250$  mm.

$$n = \frac{v_f}{\pi D} = \frac{4 \frac{m}{min}}{\pi(250 \text{ mm})} = 5.09 \text{ rpm}$$

Consulting the supplier's catalog (Catálogo motoredutores, 2007), the selected gearmotor is:

Worm drive gearmotor with crown S67DZ90S8

Type: S

Size: 67

Power: 0.37 kW

Output rotation speed: 5.2 rpm

Reduction rate (I): 158.45

Service factor (SEW  $f_e$ ): 1.35

Mass (m): 39 kg

### **Considerations**

The worm drive gearmotor with crown secures that the gearmotor is irreversible, because of the high friction among the gears and the high reductions involved. This way, it is guaranteed that the load would not face a free fall if there is an eventual lack of electric power. There is no need to use breaks.

#### 4.3.5 Steel Cable

This section was adapted from (COSTA, 2016). It will comprise all the calculations aiming the selection of the steel cable.

#### **Calculus of the theoretical force in the cable $F_0$**

The force  $F_0$  will raise the load of the vehicle on the platform. As afore calculated, the force to elevate the platform, considering only the second-class lever mechanism is,  $F = 12,579.58 \text{ N}$ .

Now considering the movable pulley as well, the force that is needed to elevate the platform is  $F_0$ , which can be calculated as:

$$F_0 = \frac{F}{2} = \frac{12,579.58 \text{ N}}{2} = 6,289.79 \text{ N}$$

### **Calculus of the real force $F_A$ necessary to elevate the load on the platform**

In the real situation there will be friction increasing the force necessary to elevate the load ( $F_0$ ) because of the losses provoked by this friction.

The friction is a function of the diameters (steel cable and pulley) and the lubrication (steel cable and bearings of the pulley).

The force  $F_A$  necessary to elevate the load on the platform can be calculated according to (PROVENZA, 1990) as shown below. Where  $n$  is the number of movable pulleys,  $K$  is a constant according to (PROVENZA, 1990) and  $F = 12,579.58 \text{ N}$  as calculated before.

$$F_A = \frac{F(1+k)^n \times K}{(1+k)^{n+1} - 1} = \frac{(12,579.58 \text{ N})(1+0.047)^1 \times 0.047}{(1+0.047)^{1+1} - 1} = 6,434.21 \text{ N} = 641.38 \text{ kgf}$$

It is important to notice that,  $F_A = 6,434.21 \text{ N} \geq F_0 = 6,289.79 \text{ N}$  because  $F_A$  takes the friction in consideration.

### **Efficiency $\eta$ to raise the load**

The efficiency of the system is represented by a number, which will be calculated in the present section. The efficiency is a direct relation between the ideal force on the cable  $F_0$  and the real one  $F_A$ . Thus, it can be calculated as:

$$\eta = \frac{F_0}{F_A} = \frac{6,289.79 \text{ N}}{6,434.21 \text{ N}} = 0.98$$

Which is a very good efficiency for the system according to (PROVENZA, 1990).

### **Calculus of the retention force $F_R$ necessary to hold the load when lowering the platform**

Opposite to what happens when the load is raised, the friction helps when the load is being lowered. According to (PROVENZA, 1990), the retention force  $F_R$  necessary to hold the load when lowering the platform can be calculated with the equation below, where  $n$  is the number of movable pulleys,  $K$  is a constant according to (PROVENZA, 1990) and  $F = 12,579.58 N$  as calculated before

$$F_R = F \frac{K}{(1 + k)^{n+1} - 1} = (12,579.58 N) \frac{0.047}{(1 + 0.047)^{1+1} - 1} = 6,145.37 N$$

### **Calculus of the speed $V_F$**

When utilizing a movable pulley there is the gain in the reduction of the forces, but there is an increase in the speed of the force that is generating the movement, in an inverse proportion.

The speed of the steel cable, generated by the gearmotor, will be directly proportional (and higher) than the effective speed of the load  $Q$ .

The speed of the steel cable  $V_F$  can be calculated with the equation below extracted from (PROVENZA, 1990), where  $n$  is the number of movable pulleys and  $V_Q = 2 \frac{m}{min}$  is the estimated speed of the load  $Q$ .

$$V_F = (n + 1)V_Q = (1 + 1)2 \frac{m}{min} = 4 \frac{m}{min} = 0.07 \frac{m}{s}$$

### **Selection of the steel cable according to DIN4130**

The selection of the steel cable was performed according to DIN4130, which recommends to use the following equation, where  $d_c$  is the diameter of the steel cable,  $K = 0.3$  is a coefficient class III according to DIN4130.



$$d_c = K\sqrt{F_A} = 0.3\sqrt{641.38 \text{ kgf}} = 7.60 \text{ mm}$$

Thus, the diameter must be bigger than 7.60 mm.

### **Selection of the steel cable according to the supplier's catalog**

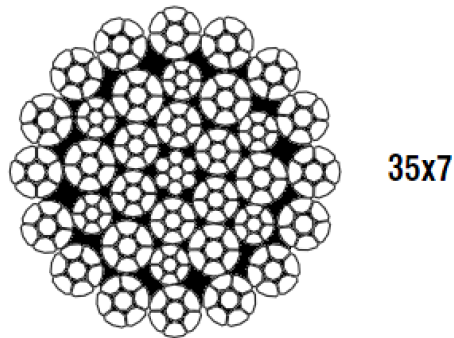
For comparison, the calculation below was executed according to the supplier's catalog (Manual Técnico de Cabos, 2009).

The work load on the steel cable CT is the real force  $F_A$  necessary to elevate the load on the platform divided by the cross section area of the estimated steel cable. In order to select the cable, the supplier's catalog recommends multiplying the CT by a service factor (SF) equal to 10 when dealing with elevators, thus calculating the minimum rupture load (CRM):

$$\text{CRM} = \text{CT} \times \text{SF} = F_A \times 10 = 641.38 \text{ kgf} \times 10 = 6.41 \text{ tf}$$

The selected steel cable must support a force equal or higher to this value in order to work securely. Figure 18 below shows the CRM values for the appropriate steel cables in the supplier's catalog. The cable with 8 mm diameter and yield strength  $E = 2,160 \frac{\text{N}}{\text{mm}^2}$  was selected.

## ErgoFlex



Diameter		Approximate Mass (kg/m)	Minimum Rupture Load (tf)	
mm	inch		1960N/mm <sup>2</sup>	2160N/mm <sup>2</sup>
8	-	0,34	6,05	6,45
9	-	0,42	7,55	8,05
10	-	0,52	9,40	9,95
11	-	0,64	11,45	12,15
12	-	0,75	13,40	14,20
13	1/2"	0,87	15,70	16,50
14	-	1,01	18,25	19,20

Figure 18 – Selection of steel cable  
Source: (Manual Técnico de Cabos, 2009) - adapted.

### Considerations

The selected steel cable must attend the two calculations, the supplier's catalog and the DIN 4130. The selected steel cable is described below and it was taken from (Manual Técnico de Cabos, 2009). As the diameter according to the supplier's catalog is bigger than 7.60 mm (DIN4130), it will work safely.

CIMAF high performance ergoflex 35x7 – 1 + 6, with the diameter of 8 mm.

#### 4.3.7 Pulley

The pulley was selected according to the steel cable. The steel cable supplier's catalog recommends a pulley that has a diameter which is at least 18 times bigger than the diameter of the steel cable, thus the diameter of the pulley  $D_p$  can be calculated as a function of the diameter of the steel cable as below.

$$D_p \geq d \times 18 \geq 8 \text{ mm} \times 18 \geq 144 \text{ mm}$$

Thus, the selected diameter for the pulley was 270 mm, which is bigger than 144 mm securing that the pulley will work safely without fail.

#### 4.3.6 Minimum diameter for the pulley's shear pin

According to the calculations on the gearmotor section, the maximal shear load on the pin of the pulley is  $F = 12,579.58 \text{ N}$ :

$$F = \frac{2565.52 \text{ kg}}{2} = 1282.76 \text{ kg} = 12,579.58 \text{ N}$$

The minimum diameter for the pulley's shear pin  $d_p$  can be calculated with the equation below, where  $\tau_c = 6.50 \frac{\text{kg}}{\text{mm}^2}$  (or  $63.74 \frac{\text{N}}{\text{mm}^2}$ ) is the permissible shear stress for the ABNT 1045 with an intermittent load according to (PROVENZA, 1990).

$$d_p = \sqrt{\frac{4F}{\pi \times \tau_c}} \Rightarrow d_p \geq \sqrt{\frac{4 \times 12,579.58 \text{ N}}{\pi \times 63.74 \frac{\text{N}}{\text{mm}^2}}} \Rightarrow d_p \geq 15,85 \text{ mm}$$

The selected diameter for the pulley's shear pin  $d_p$  is 43 mm which is bigger than 15,85 mm, meaning that it will work safely and will not suffer plastic deformation, only elastic deformation.

$$d_p = 43 \text{ mm} \geq 15,85 \text{ mm} \Rightarrow \text{ok!}$$

#### 4.3.7 Ball bearing plummer block unit

The selection of the ball bearing plummer block unit was mainly according to the shaft diameter (50 mm). The load conditions (static and dynamic) that the bearing can support is much higher than the ones to which the bearings will be submitted in the parking duplicator device. The parking devices will have two ball bearing plummer block units. The selected ball bearing was the SYJ 50 TF from the supplier SKF (Ball bearing plummer block units, 2019).

#### 4.4 **Finite Element Analysis (FEA)**

Besides the dimensioning through analytical methods, some components were also dimensioned through Finite Element Methods (FEMs) refining the calculations and validating the study. The Finite Element Analysis (FEA) was performed with the software SOLIDWORKS Simulation® and MASTAN2®. The calculations computed with the software MASTAN2® are presented along the methodology in chapter 4.3 Analytical Dimensioning. The simulations performed with the software SOLIDWORKS Simulation® and their discussion are presented in 5 RESULTS AND DISCUSSIONS.

#### 4.5 **Virtual Prototype**

The purpose of this step is to transform the generated concept into a product. It contemplates the development of a virtual prototype in the software SOLIDWORKS® v. 2019 involving each one of the equipment components, in agreement with the results of the dimensioning carried out analytically and in the Finite Element Analysis (COSTA, COSTA, *et al.*, 2017). The virtual prototype is presented in the chapter Results and Discussions.

#### 4.6 **Small-Scale 3D printed Prototype**

Based on the virtual prototype, a reduced scale prototype was 3D printed. First, a study of the 3D printing procedure was conducted, which involved the visit to 3D printing companies and the general study of the 3D printing process. Once the student understood the capabilities and limitations of the 3D printing and learned how to 3D print objects, each components of the virtual prototype was individually exported from SOLIDWORKS® v. 2019 to the format .STL. So, the components were sliced in the software Cura®, which prepares the file for the 3D

printer. The components were then finally printed in the 3D Lab Force One 3D printer. Figure 19 and Figure 20 show the 3D printer and its parameters.

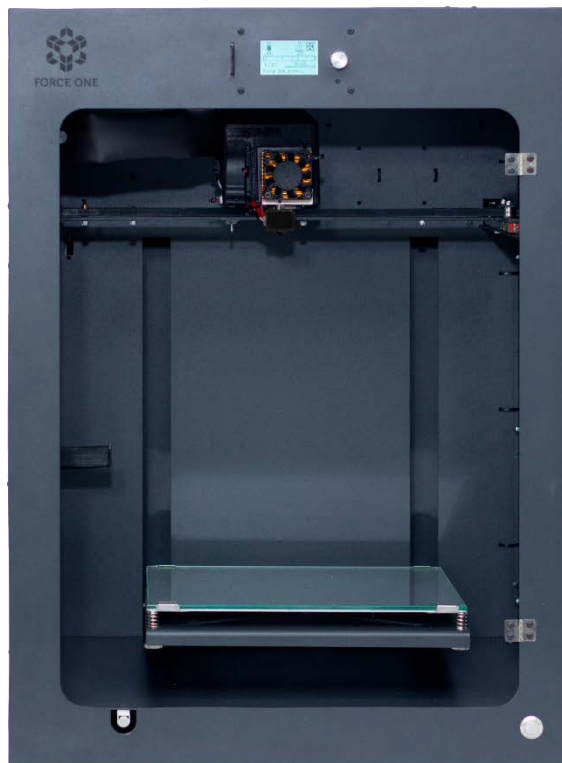


Figure 19 – Force One 3D printer of the company 3D LAB  
Source: (3D LAB, 2019).

Technical specifications		
Printing Properties	Technology	FFF (Fused Filament Fabrication)
	Printing Area	<ul style="list-style-type: none"> <li>• X = 250mm (width)</li> <li>• Y = 230mm (depth)</li> <li>• Z = 295mm (height)</li> <li>• Approximate total volume of 17 liters</li> </ul>
	External dimensions of the printer	<ul style="list-style-type: none"> <li>• W = 440mm</li> <li>• D = 405mm</li> <li>• H = 600mm</li> </ul>
	Filament Diameter	1.75mm
	Nozzle Diameter	0.4 or 0.5mm
	Layer Resolution	<ul style="list-style-type: none"> <li>• Nozzle 0.4mm = Between 50 and 300 microns (0.05 to 0.3mm)</li> <li>• Nozzle 0.5mm = Between 200 and 400 microns (0.2 to 0.4mm)</li> </ul>
	Extruder Temperature Range	Between 180 and 260°C
	Table Temperature Range	Between 30 and 115°C
	Supported Materials	PLA, ABS, ABS Premium, ABS MG94, PETG, Flexible, Nylon, Wood, HIPS, PVA, ASA, Tritan
	Noise level	Up to 50dBA
	Connectivity	USB
	Display	128 x 64
	Internal lighting	LED RGBW with color change from machine status -
	Printing table	Aluminum with glass of 4mm
	Supported Files	STL, OBJ, X3D, 3MF, BMP
	Printing Formats	GCODE, G, GCODE.gz, UFP
	Warranty Period	12 months
	Technical support	Chat, email, phone or in person

Figure 20 - Technical specifications of the Force One 3D printer  
Source: (3D LAB, 2019) - adapted.

The reduced scale 3D printed prototype served for testing. For example, in the section 4.7 Aid & Security Intelligent System, the definition of the optimal location for the sensor and cameras was done with help of the virtual prototype, where the parking maneuver was studied and the best positions were selected after evaluation. The test also proved that the device works and so validated the methodology. After tests and simulations of the device's operation with the 3D printed prototype, corrections and improvements took place in the virtual prototype. The reduced scale 3D printed prototype was also rebuilt with the developed corrections and improvements.

## 4.7 Aid & Security Intelligent System

In order to make the parking task easier, this modern vertical parking system is also equipped with a position sensor and two cameras that communicate with the driver to help him parking. The outputs from the sensor and the cameras are merged and the pose (position and orientation) of the vehicle relative to the free parking space is tracked while the car is parking. This is accomplished through an algorithm that also predicts the next pose of the vehicle based on its prior state. A small display shows the distance of the car to any object closer than 50 cm and a beep warns the driver if a collision is eminent, or if the car is oriented in a position that probably won't lead to properly parking. This technology aims the proper positioning of the vehicles while parking and the driver's safety. The present paper is focused on the development of this assistive technology. Except for the writing of the algorithm, it comprises all the steps in the conception of the aid system. On the first stage, this paper approaches the selection of the specific position sensor and cameras to be used on the parking device. The position sensor and the cameras detect with precision the position of the car and other obstacles in relation to the parking space as a function of the time as the car is parking. In the second stage, the optimal positions for the sensor and cameras were defined. On a third stage, the parking task was simulated on the software Blensor®. The obtained results were effective when applied in precisely determining the vehicle's position, assisting the driver in the task of parking and avoiding collisions.

The methodology adopted in the development of the sensor-based system aiming to facilitate the maneuvering of the car was divided in 3 steps: 4.7.1 Selection of the proper sensor and cameras; 4.7.2 Definition of the optimal location for the sensor and cameras; 4.7.3 Simulation on the software Blensor®; and 4.7.4 Development of the Algorithm. The step 4.7.4 is not concluded yet. It is important to notice that these steps did not happen linearly, they happened simultaneously or with intersection points (COSTA, VICTORINO e CHAVES, 2020).

### 4.7.1 Selection of the proper sensor and cameras

In the first step, the appropriate sensor and cameras for the presented problem were selected. The fusion of the outputs from the position sensor and the cameras must show the precise pose of the car as a function of time. Thus, the vertical parking device needs a sensor and cameras that can precisely determine the vehicles' pose throughout the entire maneuvering. At the same

time, they can't be financially expensive, as this would impair the commercialization of the device. So, in this step, the position sensors and cameras available on the market were technically and financially compared. Besides that, suchlike parking aid systems such (JUNG, CHO, *et al.*, 2008) were studied helping in the selection of the proper sensor. Simulations of various sensors and cameras took place on the software Blensor®. Thereby, the sensor and camera that offered the best benefit-cost ratio were selected (COSTA, VICTORINO e CHAVES, 2020).

#### 4.7.2 Definition of the optimal location for the sensor and cameras

In the second step, the position in which these sensor and cameras would be installed was defined. The sensor and cameras need to detect the vehicle from the start to the finish of the parking task, beginning at a distance of at least 7 meters from the device. This minimum distance is necessary so that the driver can maneuver the vehicle and get to park. The locations of the sensor and cameras were evaluated so that there were fewer obstacles between them and the vehicle. Suchlike analyzes were made through the reduced scale 3D printed prototype, which was modeled in the software SOLIDWORKS® v. 2019® and 3D printed, helping in the definition of the optimal location for the sensor and cameras.

The maneuvering of the 2 vehicles was simulated and studied on the 3D print aiming to understand the location that would make both cars (superior and inferior) be in range of the position sensor and the cameras during their whole parking task. Situations such as possible blind spots and interferences were also evaluated through this same method in this step. Thus, the optimal location for the sensor and camera was defined (COSTA, VICTORINO e CHAVES, 2020).

#### 4.7.3 Simulation on the software Blensor®

In the third step, the sensor and cameras on the parking device were simulated in the software Blensor®. First, the vertical parking device was modeled in the software SolidWorks®, then it was exported to the software Blensor®. On Blensor®, the sensor and the cameras were installed in the parking device according to the location defined on the step "B. Definition of the optimal location for the sensor and cameras". Then, the sensor and the cameras were simulated during



the maneuvering of the vehicles in the parking task. The obtained results are presented in the section of the results (COSTA, VICTORINO e CHAVES, 2020).

#### 4.7.4 Development of the Algorithm


This step isn't concluded yet. It will be presented on a future work. It consists in the development of an algorithm that will merge the data from the cameras with the information from the sensor, detecting the pose of the vehicle through corner recognition, measuring the distance from the vehicle to obstacles, interacting with the driver, avoiding collisions and assisting the driver throughout the entire task of parking. By means of Kalman Filtering (GREWAL e ANDREWS, 2001), this algorithm predicts the next pose of the vehicle based on its prior state. Also, if a person or an animal enters the parking device operational area presenting a possible injury condition, this algorithm will stop the parking device and alert the driver with a beep (COSTA, VICTORINO e CHAVES, 2020).

### 4.8 Cost Estimate

Based on the virtual prototype, a list of materials was carried out contemplating the materials and quantities necessary for the execution of the project. Through a market survey, the prices of the materials were evaluated and summed in order to obtain the manufacturing cost of the equipment considering the labor and including taxes for a proper commercialization of the parking duplicator (COSTA, COSTA, *et al.*, 2017).

First, a list of the materials was made contemplating each of the mechanical components of the parking duplicator device. This list included the dimensions of the elements and the material, which was generally the A36 steel. Once the list was created, suppliers of the mechanical components were contacted giving the price of the parts. For the labor price, i.e. the cost for the assembly of the whole device, a professional of the field was contacted and he made the cost estimate for assembling the whole device based on the developed virtual prototype as shown on Figure 21. The same was made for the folded sheet metal and all other parts, giving an accurate estimate of how much it would cost to fabricate one unit of the parking duplicator device. The price on Figure 21 is for the assembly of the whole device, including the electric engine and drive.

The result of the cost estimate is presented on section 5.5 Cost Estimate. Each element was listed with its price and the final price of the product is presented and detailed on Table 3 - Cost Estimate.



**PASSOS**  
ENGENHARIA - MG

Contagem, 25 de julho de 2019.

Proposta comercial 089/2019

Aos cuidados,  
Sr. Lucas Amaral  
[lucasac@gmail.com](mailto:lucasac@gmail.com)

1 - Objeto: Contratação de Empresa de Engenharia para montagem de dispositivo. Obra: Contagem /MG.  
2 - Validade do orçamento: 30 dias  
3 - Condição de pagamento: 100% após execução  
4 - Tempo previsto para execução da obra: 25 dias após assinatura de contrato.

**PREÇOS**

Item	Qtd.	Uni.	Descrição	R\$ Uni.	R\$ Total
1	1,00	sv	Montagem de dispositivo conforme projeto enviado.	R\$ 1.890,00	R\$ 1.890,00
<b>VALOR TOTAL</b>					<b>R\$ 1.890,00</b>
3			Tributos e impostos 14%		R\$ 264,60
<b>VALOR TOTAL GLOBAL</b>					<b>R\$ 2.154,60</b>

Sr. Lucas,

Sendo o que nos apresenta para o momento, colocamo-nos ao inteiro dispor de V. As., para quaisquer esclarecimentos que se façam necessários.

Atenciosamente,

\_\_\_\_\_  
PASSOS ENGENHARIA-MG

Razão Social: Passos J & R  
Construções e Empreendimentos Ltda.  
CNPJ - 04.352.116/0001-40  
End: Rua Delio da Consolação Rocha, 1023  
Santa Helena - Contagem - CEP: 32015-180  
[www.passosenhariaimg.com.br](http://www.passosenhariaimg.com.br)  
(31) 3044-2137 / 99786-3319

Figure 21 - Labor cost estimate.  
Source: (Passos Engenharia - MG, 2017).

## 5 RESULTS AND DISCUSSIONS

### 5.1 Virtual Prototype

The present study comprises a device for doubling garage slots composed of a lifting platform articulated on a support column and lifted/lowered by a drive assembly formed by a movable pulley and a winch (or a hoist). The Figure 22 illustrates the virtual prototype of the duplicator.



Figure 22 - Virtual prototype developed for the duplicator.  
Source: elaborated by the author.

Figure 23 shows the general operation of the proposed device: the first car is parked, lifted, and then the second car is parked below the first one. (COSTA e VICTORINO, 2019) describes its operation: “first, the superior vehicle parks over the elevating platform and the electric hoist elevates it through a steel cable and a movable pulley. Then the inferior vehicle parks under the upper one. It’s important to notice that for the superior vehicle to leave, the inferior vehicle must be removed first. Another interesting observation to be done is the fact that the elevating platform is hanging without support on one of its corners and thus this hanging platform is under a severe bending moment and requires proper dimensioning.”

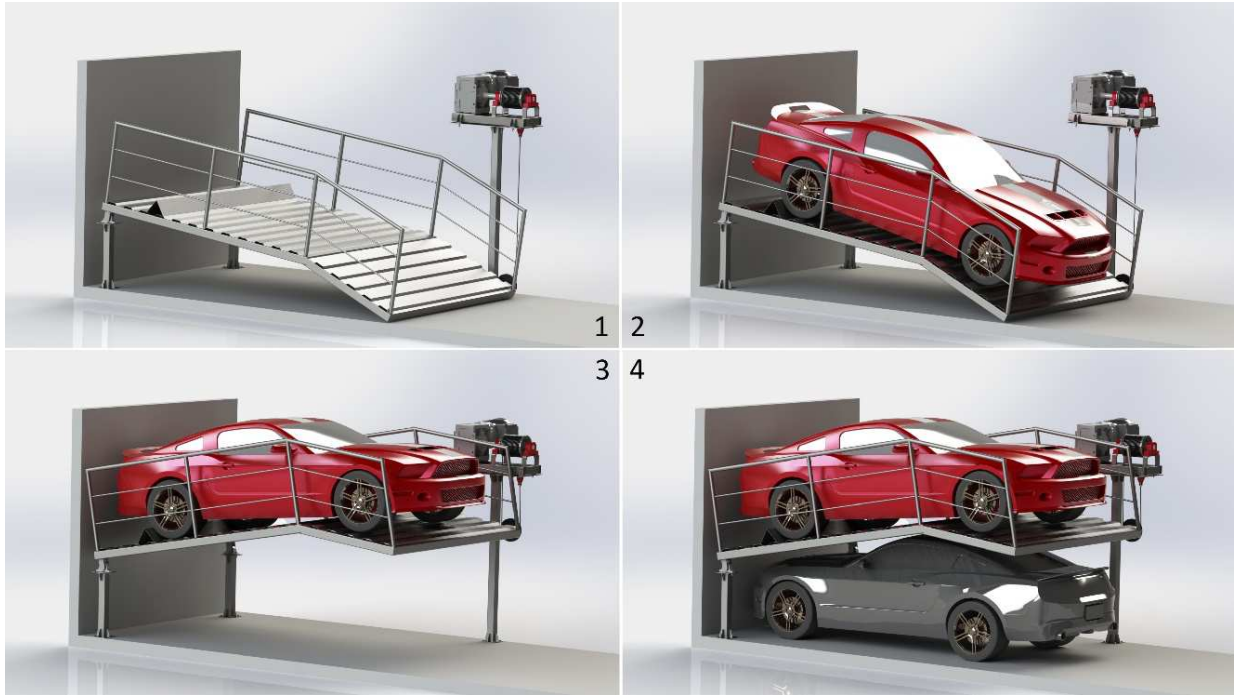


Figure 23 - Device's general operation.  
Source: (COSTA e VICTORINO, 2019).

As shown in Figure 24, the lift platform is intended to lift a vehicle and has a geometry so as to prevent any leakage of oil or water from the top vehicle to reach the bottom one. The platform has a stop in contact with which the wheels of the vehicle should be positioned when parking, preventing the raised vehicle from slipping after lifting the platform. The lifting platform is made of sheet metal which has folds that increase the mechanical resistance of the platform and thus allow the use of a thinner and therefore lighter and cheaper sheet.



Figure 24 - Parking duplicator view.  
Source: elaborated by the author.

Fig. Figure 25 shows a side view of the parking duplicator, where the two parked vehicles can be seen. The configuration described here is the basic one for the operation of the system. Other items can be added to it attempting greater security. These include: safety locks that prevent accidental lowering of the platform and miscellaneous sensors, such as those that make it impossible to lower the platform if the space below it is occupied, which interrupts the lift if the vehicle is close to touching the garage ceiling or which interrupt the operation of the platform in case a child or a domestic pet enters regions considered to be dangerous during the operation of the parking duplicator device. Other possible items are remote actuation devices, handrail on the lift platform, and protection/closure sheets for parts such as steel cable and pulley, which can injure the user in an accidental contact.



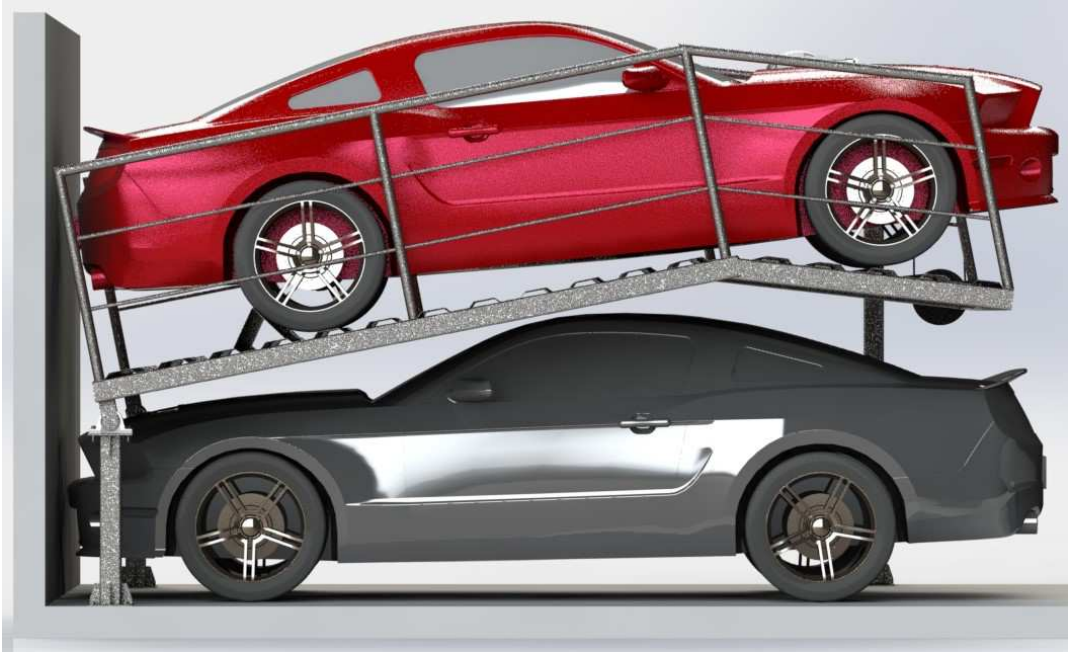


Figure 25 - Side view of the parking duplicator.  
Source: elaborated by the author.

The motorized system may also be mounted on the ceiling as shown in Figure 26, thus allowing an alternative assembly for the device.

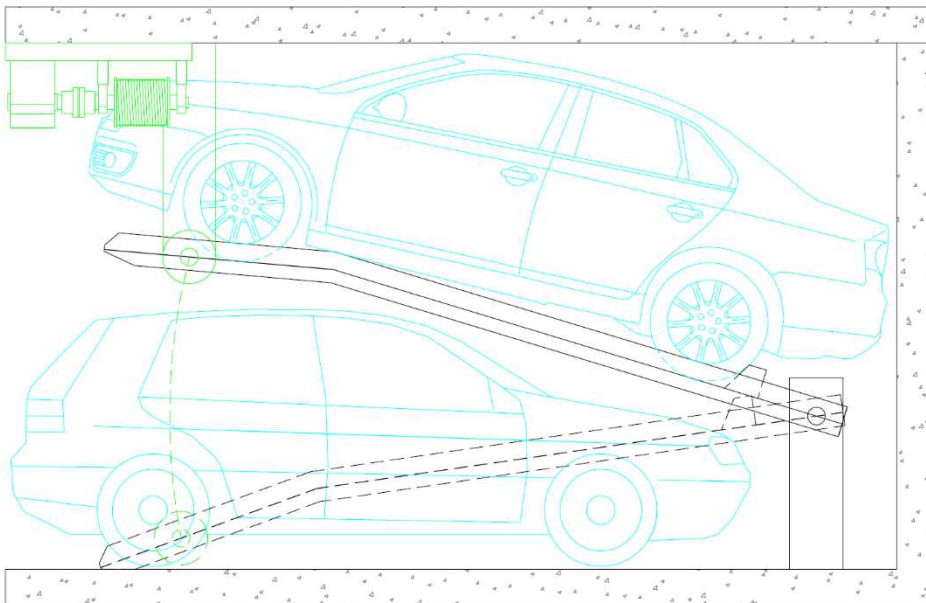


Figure 26 - Alternative assembly (dimensions in mm).  
Source: (COSTA, COSTA, *et al.*, 2017).

The obtained result was a simple device that serves as an alternative to be implemented mainly in parking lots, apartment buildings, private homes and offices. A patent application has already been properly deposited under the registration number: BR1020170118142, which enables the full commercialization of the equipment. Some important technical details of the duplicator are presented in Table 1, where it is important to notice that the height of the build must be approximately 3 m in order to properly accommodate the device:

Table 1 - Technical Details

<b>Technical Details</b>	
Motor Power	3 hp
Max. Possible Weight	2000 Kg
Height	2950 mm
Lengh	5000 mm
Width	3250 mm

SOURCE: (COSTA, COSTA, *et al.*, 2017).

Section 5.1 Virtual Prototype was adapted from (COSTA, COSTA, *et al.*, 2017), a study written by the author of this thesis.

## 5.2 Grid

The grid is the main mechanical component supporting the load when lifting the vehicle. In order to guarantee the calculations, the load on the grid was simulated in the software SOLIDWORKS® v. 2019. Figure 27 shows the bending stress ( $\text{N/m}^2$ ) acting on the grid. It is possible to see the direction of the deformation when the load is applied as a distributed load over the entire surface of the grid. All the grid is under a stress lower than the yield strength of the material ( $2.5 \times 10^8 \text{ N/m}^2$  according to the software). The simulation shows the grid mainly colored by blue, which means that these regions are far from reaching the yield strength of the material. Thus, the grid can support the load condition safely, i.e., it will not suffer plastic deformation, only the elastic one.

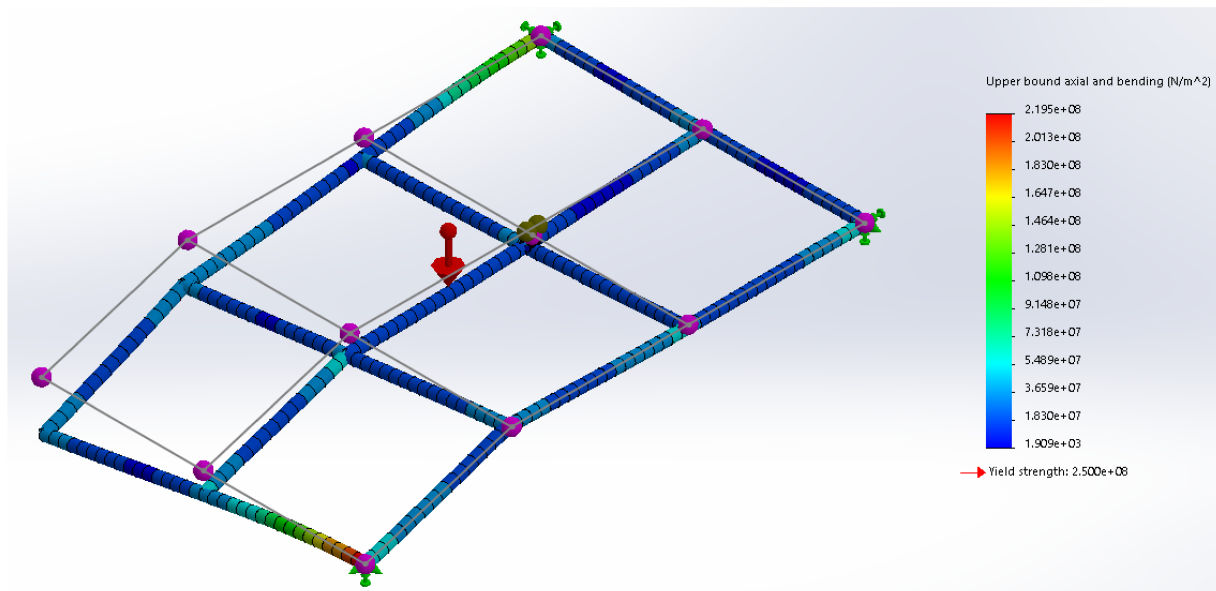


Figure 27 - Upper bound axial and bending ( $\text{N/m}^2$ ).  
Source: elaborated by the author.

The beam on the inclined portion of the grid, i.e., where there is the major deformation is colored with warmer colors. Thus, it is interesting to conduct a study with a thicker profile on this element. Figure 28 shows the Finite Element Analysis when only the front beam of the grid is replaced for a thicker profile  $100 \times 100 \times 8 \text{ mm}$ . All the other beams that constitute the grid have the profile  $100 \times 100 \times 5 \text{ mm}$ . It is possible to see a reduction of approximately 45 % in the maximal bending moment acting on the grid. Which can be a convenient way to increase the mechanical strength of the grid.



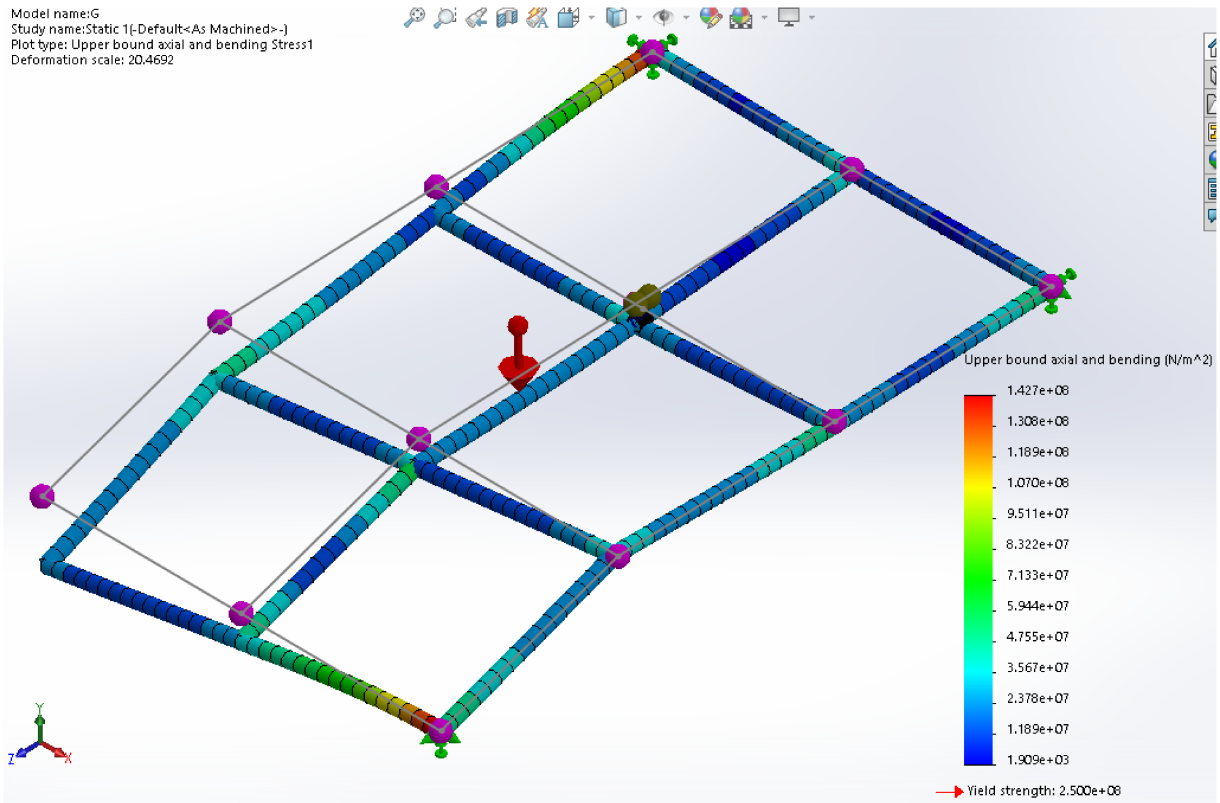


Figure 28 - FEA with a beam 100x100x8 mm

Source: elaborated by the author.

After the analytical and Finite Element Analysis, the dimensions that ensure safe operation for the grid were selected. As the 100x100x5 mm profile showed good results, it was chosen to build the grid with the reservation that only the front beam is the 100x100x8 mm profile, thus ensuring higher mechanical resistance at the low weight of steel. Figure 29 shows the main dimensions of the grid.

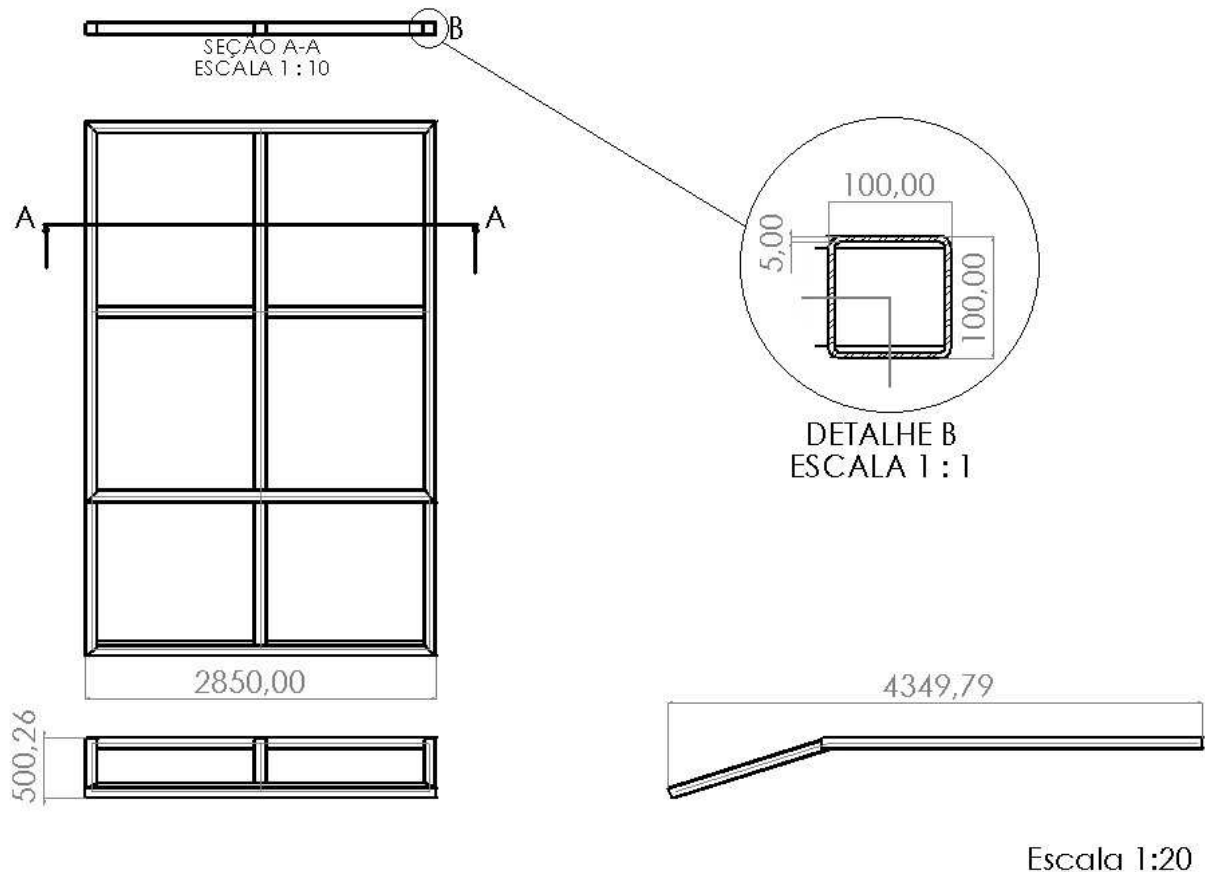


Figure 29 - Main dimensions of the grid  
Source: (COSTA e VICTORINO, 2019).

The dimension of all other parts of the parking system are presented in the detailed design in APPENDIX A - Drawing 1, APPENDIX B – Drawing 2 and APPENDIX C – Drawing 3.

## 5.2 Small-scale 3D printed Prototype

Based on the drawings, a small-scale prototype was manufactured, which served for testing and so the corrections were applied to the detailed design. The prototype was 3D printed in the scale 1:20. The very prototype was also rebuilt and so updated with the new improvements arisen from the tests. Figure 30 shows the small-scale 3D printed prototype in its most updated configuration. The prototype accordingly simulates the operation of the device. The main mechanical elements were assembled, i.e., the platform, pivots, pillar, movable pulley, gearmotor, steel cable (a nylon line in the prototype), two vehicles. The prototype operated

normally and served for the aimed purposes of testing and representing the operation of the device.



Figure 30 - Small-scale 3D printed prototype.  
Source: (COSTA, VICTORINO e CHAVES, 2020).

A mini gearmotor was installed on the prototype. Table 2 shows the technical details of the mini gearmotor.

Table 2 - Technical details of the mini gearmotor

Technical Details	
Voltage	12 V
Current at maximum load	180 mA

<b>Technical Details</b>	
Power	1.1 W
Maximum Torque	6.5 kg cm
Maximum Speed	62 rpm
Mass	170 g

SOURCE: elaborated by the author.

The gearmotor is controlled by an electronic circuit shown on Figure 31. The electric circuit is composed by the following elements: a H bridge, which switches the polarity of the voltage allowing the DC motor to run forwards or backwards; a potentiometer, allowing the adjustment of the voltage and thus allowing the adjustment of the speed of the motor, i.e., the speed in which the lift platform raises the vehicle in the parking device; a switch that can interrupt/allow the current or make the motor run forwards/backwards. It is important to notice that the potentiometer has an on-off switch as well. An AC/DC power connected to 110 V AC supplies the DC motor.

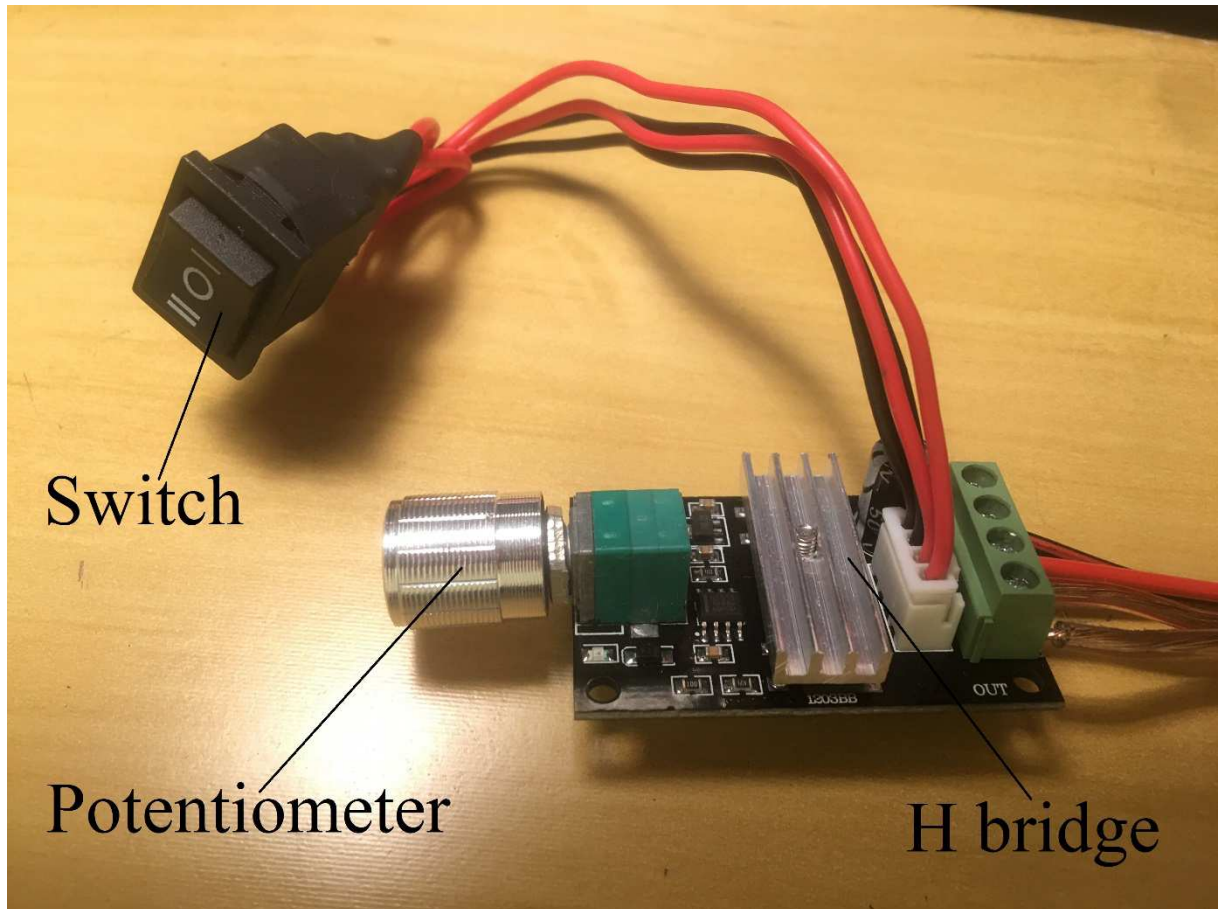


Figure 31 - Electronic circuit of the mini gearmotor.  
Source: elaborated by the author.

### 5.3 Aid & Security Intelligent System

If the upper vehicle is parked and a second vehicle hits the pillar or the pivots during its parking maneuver, a dangerous accident could occur. Thus, in the present section, technologies that communicate with the driver and help him park easily and safely have been incorporated to this device. This technology implanted in the device is composed of a position sensor and two cameras. On a first step, the proper position sensor and cameras for the problem were selected. On a second step, the optimal positions for the chosen laser sensor and cameras were defined. On a third and last step, the maneuvering of the vehicles during the parking task was simulated in the software Blensor®. The obtained results were effectively used determining the vehicle's position precisely, assisting the driver in the task of parking and avoiding collisions.

The selection of the proper sensor and cameras and the definition of its optimal location in the vertical parking have a strong influence in the efficiency of the parking task. Therefore, the results present the selection and the location of cameras and sensor which explore the maximum efficiency of the devices.

Section 5.3 (including all its subsections) was adapted from (COSTA, VICTORINO e CHAVES, 2020), a study written by the author of this thesis.

### 5.3.1 Selection of the proper sensor and cameras

Several lidar laser sensors were simulated on the software Blensor ® to defined the best one for the vertical parking. The generic lidar laser sensor with one ray that reaches 10 meters proved to be efficient in the action of detecting the position of the vehicle near the vertical parking. Besides that, it is cheap in the market of laser sensors which makes it a good option considering the benefit-cost ratio. Also, in the software Blensor ® was simulated many types of cameras to define the best one for the vertical parking. The type of camera Canon APS-C proved to be efficient in the action of detecting the position of the vehicle in relation to the time while it parks. The type Canon APS-C proved to be a good option for the device because it can see very well the space necessary for the vehicle to make maneuvers to park and it can accompany the vehicle during the entire parking task. Besides that, this type present better benefit-cost ratio than other types of camera for the needs of the device.

### 5.3.2 Definition of the optimal location for the sensor and cameras

The definition of the best location for the sensor is very important to improve sensor efficiency. After testing many places in the software Blensor ®, the best location was defined. As shown in the Fig. 3, it is located in the same column where the Eletric hoist is, and at 0.73 m above the floor. This height is ideal, because the generic lidar sensor can detect the position of the vehicle reaching more area of the vehicle than other heights. Also, the lidar sensor is installed in an angle of  $-35^\circ$  in relation to the red cartesian axis shown on Fig. 3. This angle is important, because the sensor angle together with the sensor height can properly see obstacles and detect the vehicle during the entire task of park, including within the platform. The position of the camera in the vertical parking is essential to use your maximum potential in the device. The camera was simulated in different places on the software Blensor ® and it was concluded that

the device needs two cameras. One is located in the wall at a height of 2.7 m above the floor. This height is necessary so that the camera can properly see the space available for parking when the platform not suspended. After the platform with a vehicle is suspended, the camera's vision becomes a little poor, so another camera is needed to see the other car that will park underneath. The other camera is located below the platform at a height of 0.45 m above the floor. Now, this height is necessary so that the camera can properly see the free space for parking when the platform is suspended, i.e., when the vehicle is parking in the bottom parking slot. Therefore, the two cameras are essential to the operation of the device when the platform is suspended, or when it is not. Figure 32 shows the locations of installation of the sensor and the cameras. It is possible to see that the sensor on Figure 32 is bigger than in reality, because in the software Blensor ® it is not possible to let the sensor in its original size, which would be smaller than presented on Figure 32.

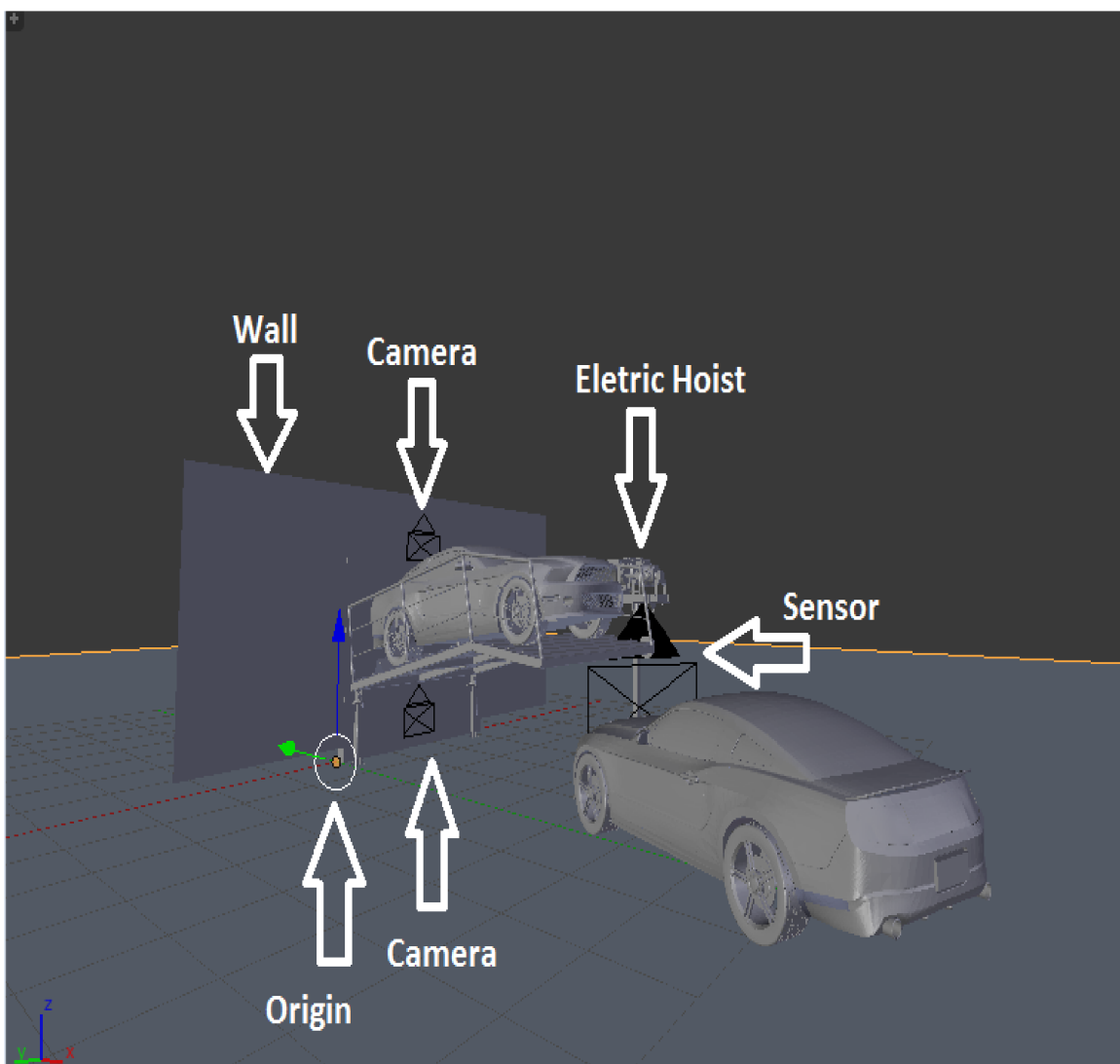


Figure 32 - Location of cameras and sensor.  
Source: (COSTA, VICTORINO e CHAVES, 2020).

### 5.3.3 Simulation on the software Blensor®

After proper selection of the sensor and cameras and definition of the optimal location them, they were simulated in the Blensor ® individually. Therefore, four images were generated on Fig. 5.3.3, two of them show the camera and sensor views. The camera view in Fig. 4 shows the simulation of the camera with excellent results, because the chosen camera can really accompany the vehicle during the entire maneuver with an accurate definition of the pose of the vehicle in the space of parking. Also, the scan view in Fig. 5.3.3 can really detect the position of the vehicle with precision in the parking area. In the image Scan View in Fig. 5.3.3, the orange line is the back of the car that is in contact with the laser. Also, it is possible to realize that a piece of the platform was detected, which was expected as the laser can reach the vehicle with precision until the very end of the parking task, when the vehicle is finally on the platform. The coordinates of the sensor view are presented on the image with the description “Location” on Figure 33, in relation to the origin presented on “General View” in Figure 33.



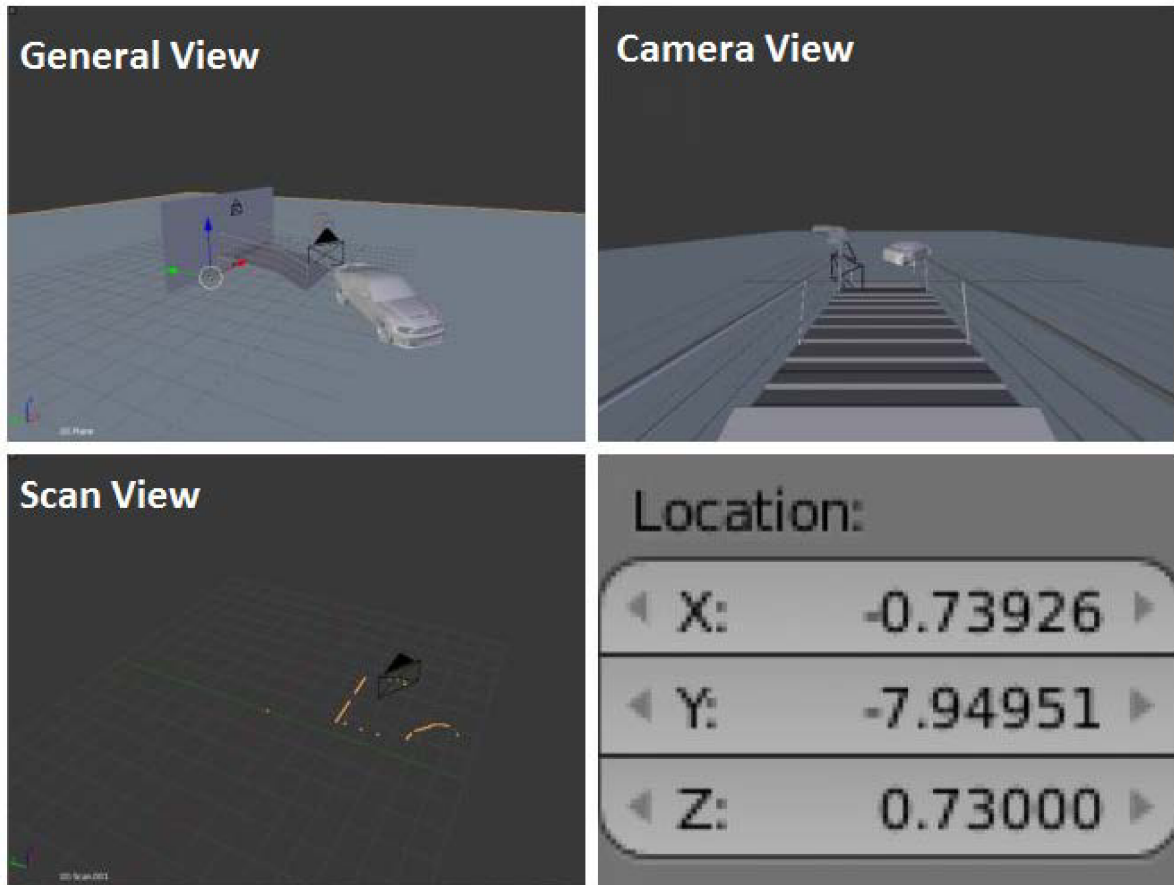


Figure 33 - Parking maneuver.  
Source: (COSTA, VICTORINO e CHAVES, 2020).

## 5.5 Cost Estimate

Table 3 shows the cost estimate for the parking duplicator device in the Brazilian coin Real while Table 4 shows it in American Dollars considering that \$1.00 = R\$4.213 (Banco Central do Brasil, 2019). After elaborating this evaluation according to section 4.8 Cost Estimate, it is estimated that the device could be marketed for R\$ 18,546.40, including manufacturing cost and taxes. It is a cheap device due to its simplicity, being cheaper than the solutions currently available in the market, which are currently commercialized for around R\$20,000 (or \$5,000), which does not count with the intelligent aid system of the present device. And the very simplicity of the designed duplicator ensures its functionality. The device also has the feature of being easily manufactured, transported and assembled in series, which provides lower final cost to the finished product.

Table 3 - Cost Estimate (R\$)

Cost Table					
Item	Unit	Quantity	Price/unit	Total Price	
Square profile 100x100x5	m	27.50	R\$ 106.91	R\$	2,939.78
Circle profile 19x0,9	m	23.43	R\$ 2.43	R\$	57.00
Circle profile 50,8x1,6	m	16.72	R\$ 10.67	R\$	178.35
Sheet metal with 2 mm of thickness	m <sup>2</sup>	14.80	R\$ 315.00	R\$	4,660.78
Sheet metal with 6,35 mm of thickness	m <sup>2</sup>	0.85	R\$ 375.00	R\$	317.91
Sheet metal with 12,70 mm of thickness	m <sup>2</sup>	0.05	R\$ 740.00	R\$	39.37
Sheet metal with 9,53 mm of thickness	m <sup>2</sup>	0.01	R\$ 550.00	R\$	5.87
Bearing	Unit	2.00	R\$ 26.52	R\$	53.04
Shear pin Ø50 of bearing	m	0.14	R\$ 150.00	R\$	21.00
Screw M16 60x60	Unit	20.00	R\$ 1.80	R\$	36.00
Screw Flange class 8	Unit	20.00	R\$ 0.47	R\$	9.40
Ferrule	Unit	20.00	R\$ 0.25	R\$	5.00
Steal cable Ø8	m	5.00	R\$ 62.39	R\$	311.95
Steal Pulley Ø160	Unit	1.00	R\$ 40.00	R\$	40.00
Shear pin Ø42,2x5 of pulley	m	0.05	R\$ 15.63	R\$	0.77
Gearmotor	Unit	1.00	R\$ 5,971.34	R\$	5,971.34
Support Gearmotor	Unit	1.00	R\$ 322.65	R\$	322.65
Lidar Sensor	Unit	1.00	R\$ 168.00	R\$	168.00
Camera	Unit	2.00	R\$ 199.00	R\$	398.00
Labor cost: 2 mm sheet folding	Unit	1.00	R\$ 855.60	R\$	855.60
Labor cost: assembly, cutting, welding	Unit	1.00	R\$ 2,154.60	R\$	2,154.60
<b>TOTAL</b>				<b>R\$</b>	<b>18,546.40</b>

Source: elaborated by the author.

Table 4 - Cost Estimate (\$)

<b>Cost Table (\$)</b>						
<b>Item</b>	<b>Unit</b>	<b>Quantity</b>	<b>Price/unit</b>		<b>Total Price (\$)</b>	
Square profile 100x100x5	m	27.50	R\$	25.38	\$	697.79
Circle profile 19x0,9	m	23.43	R\$	0.58	\$	13.53
Circle profile 50,8x1,6	m	16.72	R\$	2.53	\$	42.33
Sheet metal with 2 mm of thickness	m <sup>2</sup>	14.80	R\$	74.77	\$	1,106.28
Sheet metal with 6,35 mm of thickness	m <sup>2</sup>	0.85	R\$	89.01	\$	75.46
Sheet metal with 12,70 mm of thickness	m <sup>2</sup>	0.05	R\$	175.65	\$	9.35
Sheet metal with 9,53 mm of thickness	m <sup>2</sup>	0.01	R\$	130.55	\$	1.39
Bearing	Unit	2.00	R\$	6.29	\$	12.59
Shear pin Ø50 of bearing	m	0.14	R\$	35.60	\$	4.98
Screw M16 60x60	Unit	20.00	R\$	0.43	\$	8.54
Screw Flange class 8	Unit	20.00	R\$	0.11	\$	2.23
Ferrule	Unit	20.00	R\$	0.06	\$	1.19
Steal cable Ø8	m	5.00	R\$	14.81	\$	74.04
Steal Pulley Ø160	Unit	1.00	R\$	9.49	\$	9.49
Shear pin Ø42,2x5 of pulley	m	0.05	R\$	3.71	\$	0.18
Gearmotor	Unit	1.00	R\$	1,417.36	\$	1,417.36
Support Gearmotor	Unit	1.00	R\$	76.58	\$	76.58
Lidar Sensor	Unit	1.00	R\$	39.88	\$	39.88
Camera	Unit	2.00	R\$	47.23	\$	94.47
Labor cost: 2 mm sheet folding	Unit	1.00	R\$	203.09	\$	203.09
Labor cost: assembly, cutting, welding	Unit	1.00	R\$	511.42	\$	511.42
<b>TOTAL</b>					<b>\$</b>	<b>4,402.18</b>

Source: elaborated by the author.

## 6 NOTES

In order to prevent injuries, the grid can also be covered with a rubber protection for the areas where there is a possibility of the driver hit the head on the grid while getting in/out of the vehicle parked underneath.

The steel cable is uncovered on the virtual prototype so that the drive of the device can be exposed and properly understood. A cover constituted of a sheet metal is predicted to cover the whole drive including the movable pulley and steel cable.

As it can be seen on the drawings in the Appendix section, there is approximately 0.8 m for the driver to move to walk out of the platform after parking the upper vehicle.

The upper vehicle can be parked backwards or frontwards, but the total high of the system is generally lower when it is parked backwards.

As it can be seen in

APPENDIX A - Drawing 1, the minimal dimensions required to install the device are 5000 x 3300 x 3000 mm (length x width x high).

The pillar and the pivots are screwed on the floor.

It is possible to adapt a manual system on the gearmotor for an occasional lack of power. This manual system would be constituted of a hand crank.

## 7 CONCLUSION

At the beginning of this study, a solution was sought in saving space for parking cars. A simple and inexpensive solution to optimize parking lots, especially in parking companies and apartment buildings, where the parking space should be optimized. Analyzing the evolution of the results, we can see the relevance of the project. The device designed in this article brings a parking solution when verticalizing the use of spaces. The parking duplicator compacts parking slots offering convenience and efficient use of space. It saves time, money, space and simplifies the often tedious task of parking.

An optimization of the mechanical components of this parking duplicator was sought at the beginning of the current study and so it was performed. The designed components provide an efficient mechanical solution for the duplicator having been extensively evaluated in its maximal loading conditions in order to be dimensioned in its limit parameters minimizing the manufacturing costs and simplifying the assembly.

The stress-strain analysis of the grid was efficiently conducted with the main objective of attaining maximal equivalent stress at minimum weight. The study in the grid leads to the following conclusions. The designed architecture is an efficient choice for the parking system's grid, being capable to lift a vehicle that weighs 5.92 times the weight of its steel structure. The bending moment is the limiting strain. Once the structure is dimensioned to resist the bending moment, it will resist to all other strains. The analytical methods and the FEA Analysis effectively selected the beam with the cross-section of 100x100 mm with a wall thickness of 5,0 mm to build the grid. The beam's material is the ABNT 1045 cold rolled steel, which proved to be a good choice for the desired application.

The present paper also proposed a parking aid system able to assist the driver throughout the entire parking task in the parking duplicator. This parking aid system is composed of cameras and a laser sensor. After its development, its operation was simulated on the software Blensor®, where the cameras and sensors were evaluated. The obtained results showed that the developed system is robust. The selected sensor/cameras and their locations were able to precisely detect the vehicle throughout the entire maneuver on both parking spaces. The system can effectively warn the driver avoiding collisions and assist him through the entire task of parking. The next

step in this aid system research is the development of the algorithm that will make the fusion of the data from the sensor and the cameras, localizing the car through corner recognition, evaluating the distance of the vehicle to obstacles and interacting with the driver while assisting him.

In view of the results, it is concluded that the project conforms to the expected specifications allowing the development of a product that can be widely used in urban centers conceiving wide parking possibilities. The methodology applied in the project development of the present discussion demonstrated to be efficient and so it can be applied to the development of virtually any mechanical design. It was possible to develop a product that can be used in any urban center, opening wide parking possibilities (COSTA, 2017), (COSTA e VICTORINO, 2019), (COSTA e VICTORINO, 2018), (COSTA, COSTA, *et al.*, 2017) and (COSTA, VICTORINO e CHAVES, 2020).

## **SUGGESTIONS FOR FUTURE WORK**

For future work, the following ideas are suggested:

- The fabrication of the parking duplicator device;
- In the master's degree intelligent systems were developed to be installed in the duplicator device, facilitating the vehicle maneuver, avoiding collisions and accidents; Now, the systems to be installed in the vehicle could be developed, allowing it to maneuver autonomously, in addition to the further development of the respective systems installed in the duplicator;
- Set the tolerances and clearances of the device;

## REFERENCES

- 3D LAB. **3D LAB Soluções em Impressão 3D**, 2019. Disponível em: <<https://3dlab.com.br/>>. Acesso em: 17 August 2019.
- A proporção de habitantes por carro nas capitais. **NEXO Journal**, 1 January 2016. Disponível em: <<https://www.nexojournal.com.br/grafico/2016/01/29/A-propor%C3%A7%C3%A3o-de-habitantes-por-carro-nas-capitais>>. Acesso em: 8 August 2019.
- A36 steel. **Wikipedia**, 2019. Disponível em: <[https://en.wikipedia.org/wiki/A36\\_steel](https://en.wikipedia.org/wiki/A36_steel)>. Acesso em: 27 August 2019.
- BALL bearing plummer block units. **SKF**, 2019. Disponível em: <<https://www.skf.com/us/products/bearings-units-housings/bearing-units/ball-bearing-units/y-bearing-plummer-block-units/Y-bearing-plummer-block-units/index.html?designation=SYJ%2050%20TF&unit=imperialUnit>>. Acesso em: 3 September 2019.
- BANCO Central do Brasil. **Banco Central do Brasil**, 2019. Disponível em: <<https://www.bcb.gov.br/>>. Acesso em: 5 December 2019.
- BLENSOR. Blender Sensor Simulation. **Blensor**. Disponível em: <<https://www.blensor.org/>>. Acesso em: 17 August 2019.
- CATÁLOGO motoredutores. 08/2007. ed. [S.l.]: SEW EURODRIVE®, 2007. Disponível em: <<https://download.sew-eurodrive.com/download/pdf/10541780.pdf>>. Acesso em: 17 August 2019.
- CHAGAS, J. E. D. A. **Dispositivo para Erguer Veículos para Duplicação do Aproveitamento de Espaço em Garagens**. PI 0002843-6 A, 14 June 2000.
- COSTA, L. A. **Desenvolvimento de um Dispositivo Mecânico Elevador de Carros Objetivando Otimizar a Área Utilizada em Garagens**. Belo Horizonte: Universidade Federal de Minas Gerais, v. Bachelor's thesis, 2016.
- COSTA, L. A. **Dispositivo Duplicador de Vagas de Garagem**. BR 10 2017 011814 2, 2 June 2017.
- COSTA, L. A. et al. Development of a Parking Duplicator Mechanical Device Driven with Pulley. **Brazilian Technology Symposium (BTSym'17)**, Campinas, 2017. Disponível em: <<http://lcv.fee.unicamp.br/images/BTSym-17/Papers/72182.pdf>>. ISSN: 2447-8326.
- COSTA, L. A.; VICTORINO, A. C. Stress-Strain Analysis of a Parking System's Grid. **Brazilian Technology Symposium (BTSym'18)**, Campinas, 2018. Disponível em: <<http://lcv.fee.unicamp.br/images/BTSym18/Papers/025.pdf>>. ISSN: 2447-8326.
- COSTA, L. A.; VICTORINO, A. C. Stress-Strain Analysis and Optimization of a Parking Duplicator Hanging Grid. In: IANO, Y., et al. **Proceedings of the 4th Brazilian Technology Symposium (BTSym'18) - Emerging Trends and Challenges in Technology**. Campinas: Springer International Publishing, v. 140, 2019. p. 319-327. Disponível em: <[https://link.springer.com/chapter/10.1007/978-3-030-16053-1\\_31](https://link.springer.com/chapter/10.1007/978-3-030-16053-1_31)>. ISBN: 9783030160524.



COSTA, L. A.; VICTORINO, A. C.; CHAVES, P. A. D. Development of an Intelligent Parking Aid System. In: YUZO IANO, R. A. O. S. G. K. R. P. F. **Proceedings of the 5th Brazilian Technology Symposium: Emerging Trends, Issues, and Challenges in the Brazilian Technology**. Campinas: Springer International Publishing, 2020. Accepted paper. Expected publication to 2020.

FORD Mustang 2019. **icarros**, 2019. Disponível em: <<https://www.icarros.com.br/ford/mustang/ficha-tecnica>>. Acesso em: 20 August 2019.

GRAVINA, P. B. J. **Teoria e Calculo das Cascas Cascas de Revolução**. [S.l.]: Escolas Profissionais, 1957.

GREWAL, M. S.; ANDREWS, A. P. **Kalman Filtering: Theory and Practice Using MATLAB**. 2<sup>a</sup>. ed. [S.l.]: John Wiley & Sons, Inc., 2001. Disponível em: <[staff.ulsu.ru/semoushin/\\_index/\\_pilocus/\\_gist/docs/mycourseware/13-stochmod/2-reading/grewal.pdf](http://staff.ulsu.ru/semoushin/_index/_pilocus/_gist/docs/mycourseware/13-stochmod/2-reading/grewal.pdf)>. Acesso em: 17 August 2019.

JUNG, H. G. et al. Scanning Laser Radar-Based Target Position Designation for Parking Aid System. **IEEE Transactions on Intelligent Transportation Systems**, 9, 20 May 2008. 406 - 424. Disponível em: <<https://ieeexplore.ieee.org/abstract/document/4524998>>. Acesso em: 17 August 2019.

JUNIOR, H. D. F. L.; ALENCAR, C. T. D.; JOHN, V. M. **Evolution of Space for the Automobiles in Relation to the Total Built Area of the Buildings from São Paulo**. São Paulo: Latin America Real State Society (LARES). September 2011. p. 1-18.

KUO, Z.-S. **Double-Story Parking Apparatus Having Telescopic Access**. US 5110250 A, 18 December 1990.

LEVER. **wikipedia**, 2019. Disponível em: <<https://en.wikipedia.org/wiki/Lever>>. Acesso em: 4 September 2019.

MANUAL Técnico de Cabos. Osasco: CIMAF, 2009.

PASSOS Engenharia - MG. **Passos Engenharia MG**, 2017. Disponível em: <<http://www.passosengenhariamg.com.br/index.html>>. Acesso em: 25 July 2019.

PERTENCE, A. E. D. M. Tabela de Bach. **Laboratório de Projetos Mecânicos**, 2019. Disponível em: <<https://sites.google.com/site/labprojmec/materiais/tabela-de-bach>>. Acesso em: 4 September 2019.

PROVENZA, F. **Projetista de Máquinas**. 71<sup>a</sup>. ed. São Paulo: F. Provenza, 1990. 486 p.

PULLEY. **wikipedia**, 2019. Disponível em: <<https://en.wikipedia.org/wiki/Pulley>>. Acesso em: 4 September 2019.

RIBEIRO, C. F. D. V.; ALBUQUERQUE, C. D. **Dispositivo Duplicador de Vagas de Garagem**. PI 9906103-1 A, 18 November 1999.

STRESS-STRAIN-CURVE. **simsolid**. Disponível em: <<https://www.simsolid.com/wp-content/uploads/2017/10/stress-strain-curve.jpg>>. Acesso em: 4 September 2019.

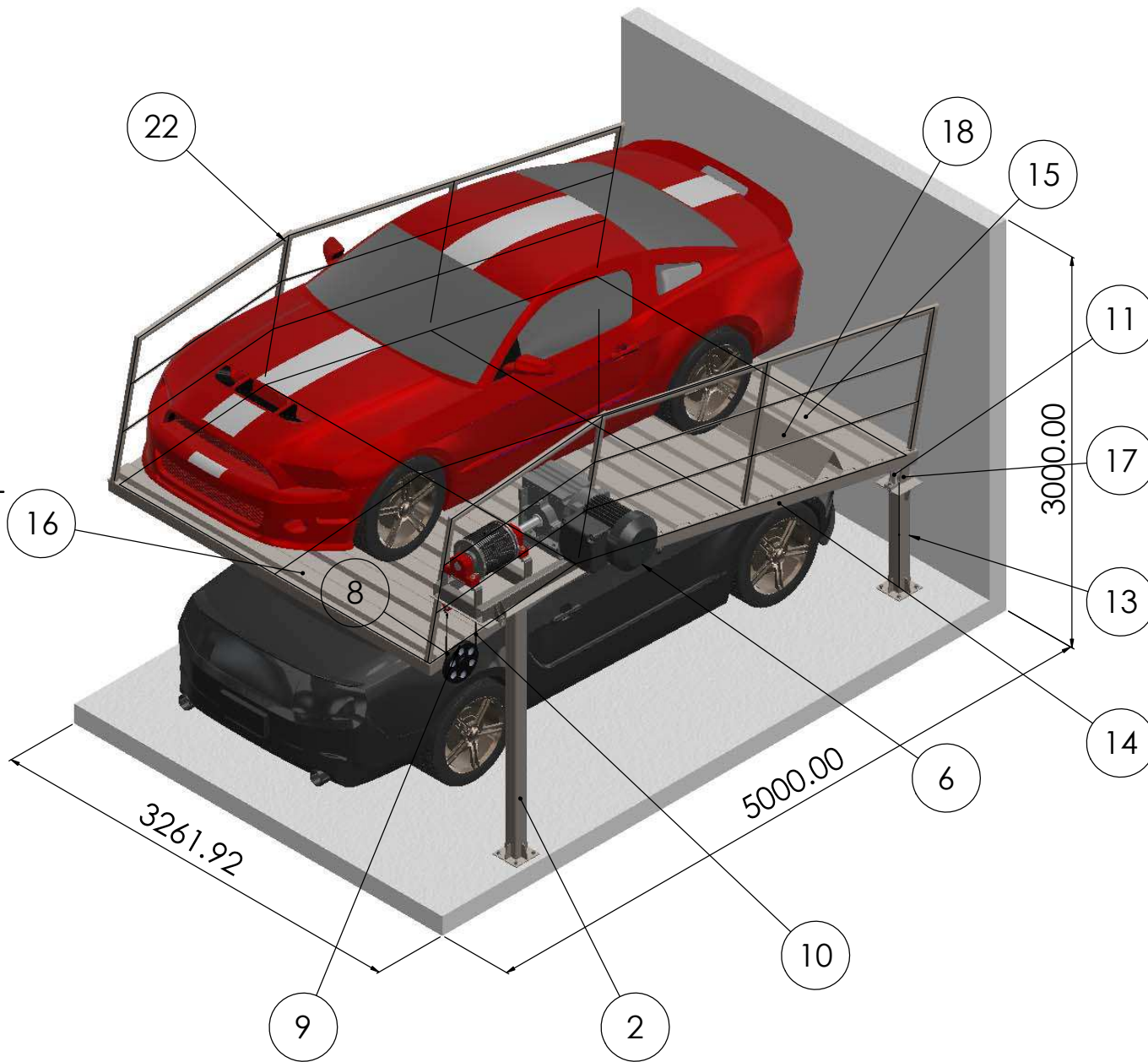
TUBOS Estruturais: Seção Circular, Quadrada e Retangular. [S.l.]: Vallourec, 2019.

VIRGINIA, U. O. Compression Elements: Buckling. **virginia.edu**, 2010. Disponível em: <<http://web.arch.virginia.edu/~km6e/arch324/content/lectures/lec-13/review-of-12.html>>. Acesso em: 27 August 2019.

WIKIPEDIA. **Statically indeterminate**, 2019. Disponível em: <[https://en.wikipedia.org/wiki/Statically\\_indeterminate](https://en.wikipedia.org/wiki/Statically_indeterminate)>. Acesso em: 12 December 2019.

WRITING A THESIS AS A COLLECTION OF PAPERS. **University of Reading**, 2016. Disponível em: <<https://www.reading.ac.uk/web/files/graduateschool/gradschwritingthesisascollectionofpapers.pdf>>. Acesso em: 17 August 2019.

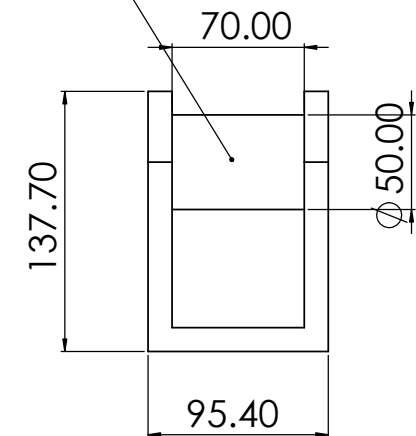
YIELD (engineering). **wikipedia**, 2019. Disponível em: <[https://en.wikipedia.org/wiki/Yield\\_%28engineering%29](https://en.wikipedia.org/wiki/Yield_%28engineering%29)>. Acesso em: 4 September 2019.



ITEM NO.	PART NUMBER	DESCRIPTION	QTY.
2	PILLAR		1
4	PEÇA23		1
6	GEARMOTOR		1
8	PULLEY's SHERAR PIN		1
9	PULLEY		1
10	STEEL CABLE		1
11	BEARING		2
13	PIVOT		2
14	GRID		1
15	SHEET METAL1		1
16	SHEET METAL2		1
17	BEARING'S SHEAR PIN		2
18	STOP		1
22	RAILING		2

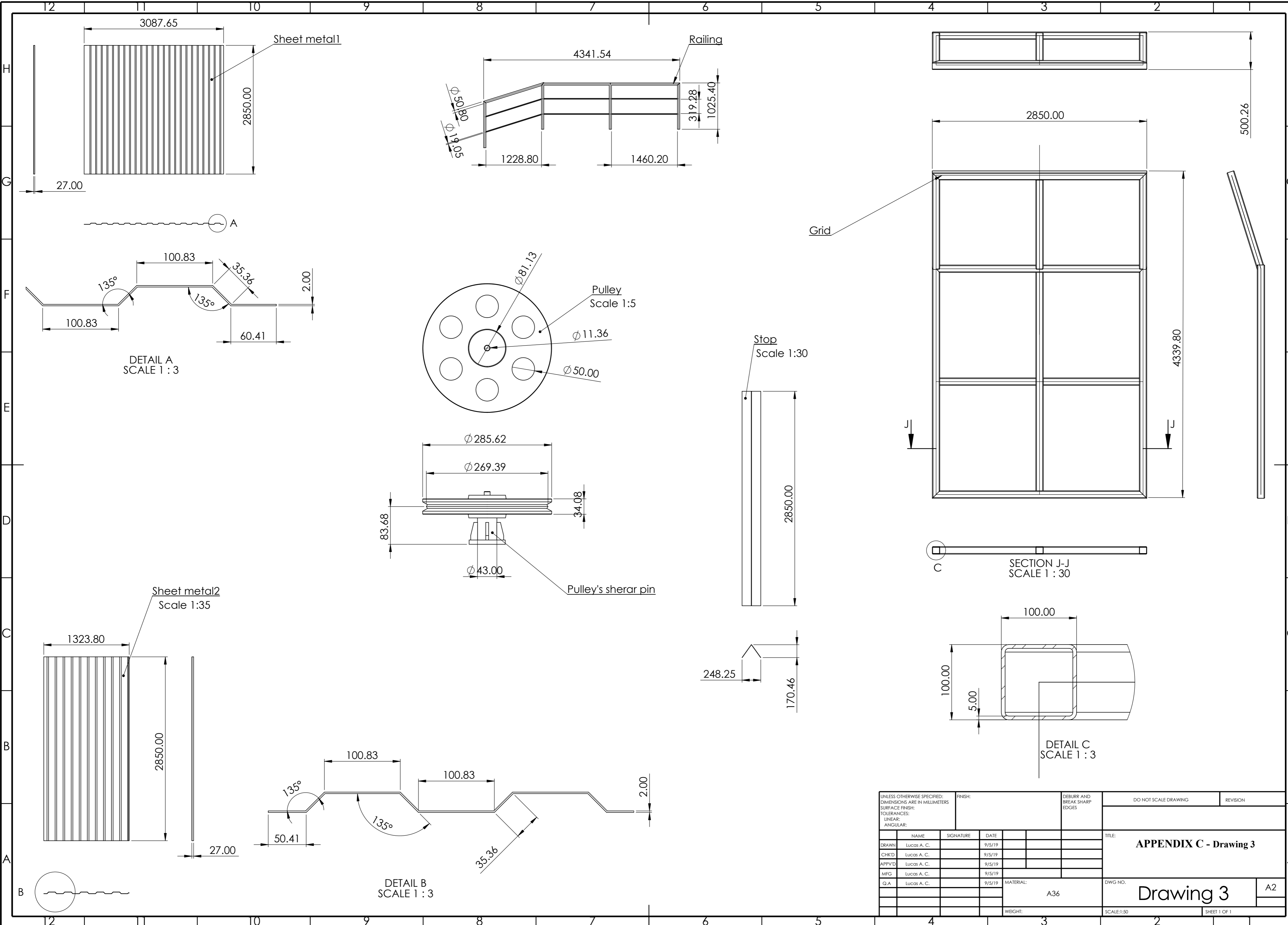
Bearing's shear pin

Scale 1:2



UNLESS OTHERWISE SPECIFIED: DIMENSIONS ARE IN MILLIMETERS			FINISH:		DIBLUR AND BREAK SHARP EDGES		DO NOT SCALE DRAWING		REVISION	
SURFACE FINISH:										
TOLERANCES:										
LINEAR:										
ANGULAR:										
NO.	NAME	SIGNATURE	DATE				TITLE: APPENDIX A - Drawing 1			
1	LUCCI A. C.		9/5/19							
2	LUCCI A. C.		9/5/19							
3	LUCCI A. C.		9/5/19							
4	LUCCI A. C.		9/5/19							
5	LUCCI A. C.		9/5/19							
6	LUCCI A. C.		9/5/19							
			MATERIAL:		A36		DWG. NO.		Drawing 1	
			WEIGHT:				SCALE:1:100		SHEET 1 OF 1	





UNLESS OTHERWISE SPECIFIED: DIMENSIONS ARE IN MILLIMETERS				FINISH:		DEBURR AND BREAK SHARP EDGES		DO NOT SCALE DRAWING		REVISION	
SURFACE FINISH:				TOLERANCES:		LINEAR:		ANGULAR:		TITLE:	
DRAWN Lucas A. C.				SIGNATURE		DATE		MATERIAL:		APPENDIX C - Drawing 3	
CHKD Lucas A. C.				DATE		MATERIAL:		DWG NO.		Drawing 3	
APPVD Lucas A. C.				DATE		MATERIAL:		SCALE:1:30		A2	
MFG Lucas A. C.				DATE		MATERIAL:		WEIGHT:		SHEET 1 OF 1	
Q.A Lucas A. C.				DATE		MATERIAL:		WEIGHT:		SHEET 1 OF 1	